Title

Hindlimb Somatosensory Information Influences Trunk Sensory and Motor Cortices to Support Trunk Stabilization.

Journal

Cerebral Cortex, 31(11)

ISSN

1047-3211

Authors

Nandakumar, Bharadwaj
Blumenthal, Gary H
Pauzin, Francois Philippe
et al.

Publication Date

2021-10-01

DOI

10.1093/cercor/bhab150

Peer reviewed

Cerebral Cortex, November 2021;31: 5165–5187

https://doi.org/10.1093/cercor/bhab150
Advance Access Publication Date: 24 June 2021
Original Article

ORIGINAL ARTICLE

Hindlimb Somatosensory Information Influences Trunk Sensory and Motor Cortices to Support Trunk Stabilization

Bharadwaj Nandakumar[1,2,†], Gary H. Blumenthal[1,2,†], Francois Philippe Pauzin[2] and Karen A. Moxon[1,2,3]

[1]Department of Biomedical Engineering, Science, and Health Systems, Drexel University, Philadelphia, 19104 PA, USA, [2]Department of Biomedical Engineering, University of California, Davis, 95616 CA, USA and [3]Center for Neuroscience, Davis, 95618 CA, USA

Address correspondence to Karen A. Moxon, University of California, Davis, 451 E. Health Sciences Drive, GBSF 3321, Davis, CA 95616, USA. Email: moxon@ucdavis.edu

[†]Bharadwaj Nandakumar and Gary H. Blumenthal contributed equally.

Abstract

Sensorimotor integration in the trunk system is poorly understood despite its importance for functional recovery after neurological injury. To address this, a series of mapping studies were performed in the rat. First, the receptive fields (RFs) of cells recorded from thoracic dorsal root ganglia were identified. Second, the RFs of cells recorded from trunk primary sensory cortex (S1) were used to assess the extent and internal organization of trunk S1. Finally, the trunk motor cortex (M1) was mapped using intracortical microstimulation to assess coactivation of trunk muscles with hindlimb and forelimb muscles, and integration with S1. Projections from trunk S1 to trunk M1 were not anatomically organized, with relatively weak sensorimotor integration between trunk S1 and M1 compared to extensive integration between hindlimb S1/M1 and trunk M1. Assessment of response latency and anatomical tracing suggest that trunk M1 is abundantly guided by hindlimb somatosensory information that is derived primarily from the thalamus. Finally, neural recordings from awake animals during unexpected postural perturbations support sensorimotor integration between hindlimb S1 and trunk M1, providing insight into the role of the trunk system in postural control that is useful when studying recovery after injury.

Key words: dermatome, dorsal root ganglion, mapping, motor cortex, sensory cortex

Introduction

Transmission of information between somatosensory and motor systems, or sensorimotor integration, is crucial for perception (Mao et al. 2011) and volitional control of movement (Rossignol et al. 2006). Understanding the substrates of sensorimotor integration is important for studies examining locomotor function. For example, sensorimotor integration has been extensively studied in the rodent whisker system (Farkas et al. 1999; Ferezou et al. 2007; Chakrabarti et al. 2008; Megevand et al. 2009; Mao et al. 2011; Hooks et al. 2013; Smith and Alloway 2013) giving rise to a better understanding of how rodents use their whiskers optimally to navigate and discriminate features of their environment. Furthermore, research on the forelimb (Asanuma et al. 1968; Chapin 1986; Tutunculer et al. 2006; Morales-Botello et al. 2012; Kunori and Takashima 2016) and hindlimb systems (Hall and Lindholm 1974; Donoghue et al. 1979; Hummelsheim and Wiesendanger 1985; Ghosh et al. 2009; Kao et al. 2009) has highlighted the importance of sensorimotor integration for appropriate locomotor function. These studies found extensive integration between anatomically and topographically corresponding sensory and motor cortices, with little cross-region integration (e.g., integration

between whisker sensory and hindlimb motor cortices). Yet, little is known about sensorimotor integration within the trunk cortex or between the trunk motor cortex and other sensory cortices, which can be of fundamental importance for studies examining learning and recovery after neurological injury or disease.

Classic mapping studies of the rodent primary sensory cortex (S1) and primary motor cortex (M1) have roughly outlined the location and border of trunk S1 and M1 (Welker 1971; Hall and Lindholm 1974; Chapin and Lin 1984). More recently, subregions of trunk S1 have been identified, including a ventral trunk representation (Xerri et al. 1994; Seelke et al. 2012) and a genital representation (Lenschow and Brecht 2018). Despite these findings, the internal somatotopy of trunk S1 remains ill defined, in part, due to the limited assessment of spinal dermatomes of the thoracic regions (Lombard et al. 1979; Takahashi et al. 1994). Similarly, trunk M1 is mentioned in most mapping studies (Donoghue and Wise 1982; Gioanni and Lamarche 1985; Neafsey et al. 1986) and some information has emerged from recent studies examining cortical reorganization after spinal cord injury (Giszter et al. 1998, 2008; Tandon et al. 2013; Oza and Giszter 2014, 2015; Ganzer et al. 2016; Manohar et al. 2017). However, little is known about the internal somatotopy of trunk M1 (Giszter et al. 2008; Tandon et al. 2013; Oza and Giszter 2015; Ganzer et al. 2016). Further study of the somatotopy of trunk S1 and M1, as well as how these cortices integrate information, is needed to understand the role of trunk cortex more fully, both in intact animals and animals that have neurological injury or disease.

Thus, the aims of the current study were to define the somatotopy of trunk S1 and trunk M1 and examine sensorimotor integration of trunk cortex. First, to examine the internal organization of trunk S1, electrophysiological mapping was performed at the spinal level to identify thoracic dermatomes and their corresponding representation in S1. Similarly, intracortical microstimulation (ICMS) was used to examine the extent and internal organization of trunk M1. Then, sensorimotor integration was assessed by examining somatosensory evoked potentials (SEPs) across broad regions of sensorimotor cortex and retrograde tracing was performed to understand the source of somatosensory input to trunk M1. Finally, to understand the functional role of sensorimotor integration, single neuron activity was recorded from trunk S1 and M1 in response to unexpected postural perturbations while animals stood on a tilting platform. Results from mapping studies reveal an important somatotopic organization within both the trunk S1 and M1 cortices. Furthermore, there is extensive sensorimotor integration between trunk and hindlimb systems, compared to the relatively weak integration within trunk and between trunk and forelimb cortices. Evidence from response latency and tracing studies suggest that this trunk/hindlimb sensorimotor integration is mediated predominately by thalamocortical projections. Importantly, this integration of hindlimb somatosensory information with trunk M1 is activated during postural adjustments to allow the animal to stabilize the trunk and maintain balance. These insights into trunk sensorimotor organization enhance our understanding of how information is processed during postural control and thereby inform the development of effective rehabilitative strategies after spinal cord injury.

Materials and Methods

Subjects

One hundred and six adult, female Sprague Dawley rats (225–250 g; Envigo) were maintained on a 12/12-hour light/dark cycle with ad libitum food and water. Fifteen animals were used to map the representation of each thoracic dermatome at the spinal level, 40 animals were used to map the internal representation of trunk S1, 21 animals were used to examine the movement representation of trunk M1, 14 animals were used to examine the integration of somatosensory information within and between sensory and motor cortices, 5 animals were used for anatomical tracing, and 11 animals were used to study sensorimotor integration relevant for postural control.

For all anesthetized experiments, animals were secured on a stereotaxic frame (Neurostar, Sindelfingen, Germany) and body temperature was maintained at 37°C using a temperature-controlled heating pad (FHC Inc., Bowdoin, ME, USA). In addition, heart rate, SpO_2, and anesthetic state (whisking/toe pinch reflex/corneal reflex) were constantly monitored. All experimental procedures were approved by UC Davis or Drexel University IACUCs and followed NIH guidelines.

Body Grid System to Map Receptive Fields

To identify receptive fields (RFs) consistently across animals, a standardized grid was outlined on each animal's dorsal trunk (Blumenthal et al. 2021). The dorsal trunk was shaved and a grid of 128 equally spaced squares was drawn indelibly. The grid spanned from the skull's base, parallel to the intertragic notch of the ear, to the tail's base (16 grids in the rostrocaudal [RC] orientation), and from the dorsal trunk's midline to its lateral aspect at the base of the limbs on each side of the animal (8 grids in the mediolateral [ML] orientation; Fig. 1A). Each grid square was approximately 1 cm^2 and was consistent across animals due to the similarity of both size and weight. In addition, a photograph of the animal with the drawn grid was taken to assist in defining RFs during S1 mapping experiments (Supplementary Fig. 2).

Mapping Thoracic Dermatomes

Animals were anesthetized with urethane (1.5 g/kg, IP) and maintained at Stage III-3 anesthesia (Friedberg et al. 1999). An incision was made along the midline of the trunk and axial musculature was separated from the vertebral column to expose the thoracic vertebrae. The spinous processes, lamina, and transverse processes of the selected thoracic vertebrae were carefully removed to access the dorsal root ganglion (DRG) on one side of the body. The animal's spinal column was secured in place by attaching locking forceps to the transverse process rostral to the T1 vertebrae and caudal to the T13 vertebrae. A single high-impedance (4–10 MΩ) tungsten microelectrode (FHC Inc., Bowdoin, ME, USA) was attached to the stereotaxic manipulator and a ground wire was placed in contact with the body cavity. The electrode was positioned over a single DRG and lowered slowly until a single cell was identified. The neuronal signal (digitized at 40 kHz) was amplified (20 000×), band pass filtered (150–8000 Hz; Plexon Inc., Dallas, TX, USA) and monitored with an oscilloscope and through audio speakers. The cell's RF was then identified using light tactile stimulation (Chapin and Lin 1984; Chapin 1986). First, the dorsal cutaneous surface of the animal

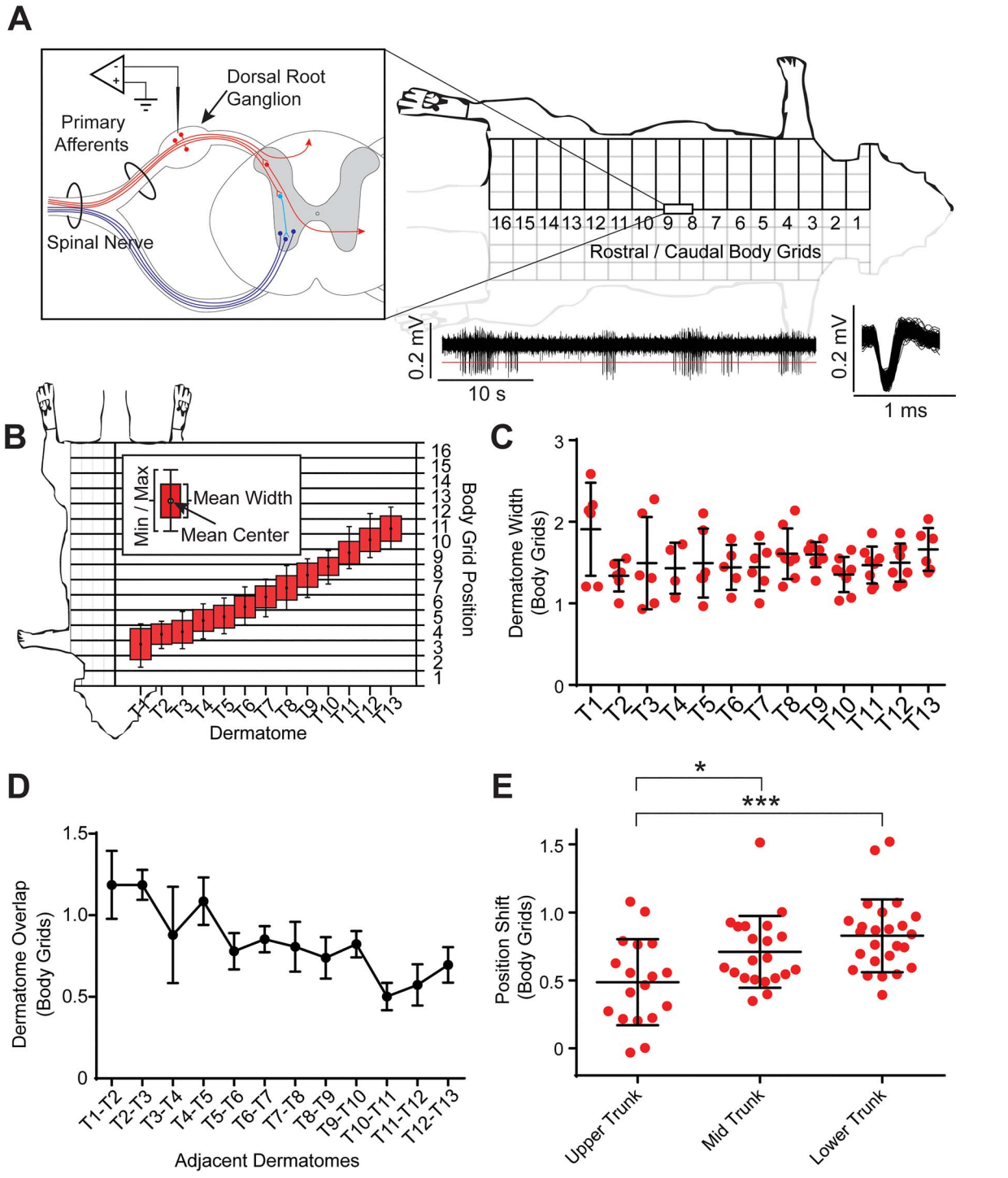

Figure 1. Trunk spinal dermatomes. (A) Dermatome map methodological diagram. A tungsten microelectrode was inserted into an average of 6 ± 3 thoracic level dorsal root ganglions (DRGs) per animal ($N = 15$), to record from primary afferent cell bodies and identify their receptive fields ($N = 86$). An example of a continuous neural trace is shownin the bottom right. (B) Average dermatome width in body grid units (each grid unit is approximately 1 cm^2) and center position plotted along the rostrocaudal axis of the body. The error bar represents the most rostral and the most caudal body grid positions of each dermatome across all animals. (C) Average dermatome width is similar throughout the rostrocaudal axis. (D) Average overlap between adjacent dermatomes showed a shift in the rostrocaudal axis. (E) Average distance in between neighboring dermatomes within the upper (T1–T5), mid (T5–T9), and lower (T9–T13) thoracic dermatomes showed a shift in the rostrocaudal axis, with a significant difference for the average distance in between neighboring dermatomes between upper trunk and mid trunk and between upper trunk and lower trunk.

was tapped with a cotton brush, both within and outside the body grid to gain insight of the neuron's RF. If the RF was located within the trunk body grid, it was then mapped with a 0.25 body grid square resolution by applying light tactile stimulation to the cutaneous surface using a wooden probe (4 mm diameter). If the RF was found outside the grid, it was not included in the mapping of thoracic dermatomes. When mapping of that neuron's RF was complete, the electrode was lowered at least 50 µm dorsoventral (DV) before another cell was identified to ensure that the same cell was not mapped twice. This process was repeated until the electrode punctured through the entire DRG. Each DRG was sampled at least three times, so as to cover the DRG's RC extent (Wessels et al. 1994). A trunk dermatome was defined as the union of all trunk grid locations on the skin that were found to be responsive to at least one cell in the respective DRG. The width of a dermatome was defined as the number of trunk grid locations within its RC extent. Center position of a dermatome was defined as the center of this RC extent. Dermatomal overlap was defined between 2 adjacent dermatomes as the distance between the rostral extent of the more caudal dermatome and the caudal extent of the more rostral dermatome.

Mapping Trunk Sensory Cortex

Animals were anesthetized with urethane (1.5 g/kg, IP) and maintained at Stage III-3 anesthesia (Friedberg et al. 1999). A craniotomy was performed on the right hemisphere to expose hindlimb S1 (HLS1), trunk S1 (TrS1), and parts of forelimb S1 (FLS1; Chapin and Lin 1984; Leergaard et al. 2004). Based on a pilot study ($n = 3$), 80 predefined cortical locations relative to Bregma were chosen. They extended from −2.0 mm to −3.8 mm RC with a resolution of 0.2 mm, and from 2.0 mm to 3.75 mm ML with a resolution of 0.25 mm between locations. At each location, the electrode was slowly lowered into the brain, up to a depth of −2.0 mm DV, while light tactile stimulation was applied to the cutaneous surface of the trunk. If a neuron was responsive, the neuron's RF was categorized into either trunk, ventral trunk, head/face, forelimb, hindlimb, tail, or a combination of body parts. If the RF included the trunk, the RF was further analyzed relative to the body grid with a 1.0 body grid square resolution and calculated separately for the supragranular, granular, and infragranular layers. A somatotopic map of the trunk and surrounding somatosensory cortices was constructed. At each cortical location, the proportion of cells that responded to each body part was investigated. A body part was assigned to a cortical location if at least 25% of the neurons in that location were responsive to that body part. If there were multiple body parts that meet the criterion, the body part with the highest proportion of responsive neurons was assigned (Fig. 2B).

To locate the cortical representation of the thoracic dermatomes within TrS1, all cells that had RF centers within trunk were used. For a given cortical location, the RC positions of the RF centers on the body grid from all cells of that location were averaged. The dermatome with the closest center position to the average cortical RF position defined the corresponding dermatome of that cortical location. Cortical locations that represented the same dermatome were grouped to generate the representation of thoracic dermatomes in the cortex. All RFs belonging to the same dermatome representation were used to calculate the amount of overlap between the neighboring dermatome representations. To analyze the size and extent of trunk RFs, only neurons that were completely contained within the borders of the trunk grid were used. Average RF size was calculated by averaging the number of responsive body grid squares for all cells.

Local Field Potential Recording in Response to Peripheral Electrical Stimulation

Electrical stimulation was chosen to compare the S1 and M1 responses to stimulation across the hindlimb, forelimb, and trunk. First, bipolar electrodes placed in the hairy skin of the hindlimb, forelimb, and trunk, were used to activate afferents between the 2 poles of the electrode. Second, to ensure fair comparisons across stimulus locations, the response of HLS1, FLS1, and TrS1 to stimulation of their RF centers was titrated to produce similar magnitudes of response across the three sensory cortices. This would be difficult to accomplish with other stimulation modalities. Although mixing of tactile and proprioceptive afferent activation cannot be ruled out, a low-intensity stimulus (0.5 mA) was used to predominantly activate tactile receptors between the 2 poles of the electrode, whereas a high-intensity stimulus (5.0 mA) was used to elicit muscle twitches and slight movements that further activate proprioceptive afferents and nociceptive afferents (Lilja et al. 2006; Yagüe et al. 2014). This higher amplitude stimulus was necessary to identify sensory responses in trunk M1. Specifically, bipolar stimulating electrodes were inserted subcutaneously into the dorsal hairy skin at four locations: hindlimb (HL), forelimb (FL), T4–T5 dermatome of the upper trunk (UT), and T9 dermatome of the mid trunk (MT; approximately the midpoint of the trunk between the FL and HL), contralateral to the recording location (Fig. 3A, Supplementary Fig. 2A). For the trunk locations, the bipolar electrodes were placed approximately 5 mm apart from each other and approximately 20 mm from the midline of the animal (approximately halfway between the midline and the grid line border of the ventral trunk). Electrical stimulation, consisting of 100 pulses (1 ms duration) was delivered every 2 s at varying stimulation intensities (see Results).

To record local field potentials (LFPs), animals were anesthetized with urethane (1.5 g/kg, IP). A craniotomy was performed on the right hemisphere to expose the sensory and motor cortices. A 32-channel, 4 shank recording electrode array (A4×8–5 mm-200-400-177; NeuroNexus, Ann Arbor, MI) was positioned over the fixed locations either spanning M1 (−3.2 to 1.2 mm RC, 1.25 mm ML), TrS1 (−3.4 mm to −2.2 mm RC, 3 mm ML), HLS1 (−1 mm to −2.2 mm RC, 2.5 mm ML), or FLS1 (0.5 mm to −0.7 mm RC, 3.5 mm ML). The array was lowered perpendicularly into the cortex to a depth of 1.8 mm where it was fixed in place.

The extracellular LFP was acquired simultaneously from all 32 channels (Intan Technologies, Los Angeles, CA, USA), digitized at 20 kHz, amplified (192×) and band pass filtered (0.1 Hz–7.5 kHz). To ensure fair comparisons between the stimulation responses of different locations on the body, the responses of each region to stimulation of their RF centers were compared (RF center identified using light tactile stimulation, see above). A high pass filter of 5 Hz was used to mitigate slow wave activity that developed under urethane anesthesia (Clement et al. 2008; Humanes-Valera et al. 2013) in the cortical LFP. A window of 1 s centered on the stimulation time was extracted from the high pass filtered LFP data (5 Hz, Butterworth order 2, zero-lag) of each recording site. The data in that window were then averaged across stimulation trials to obtain the SEP. A representative channel from the supragranular (400 µm DV), granular (800 µm

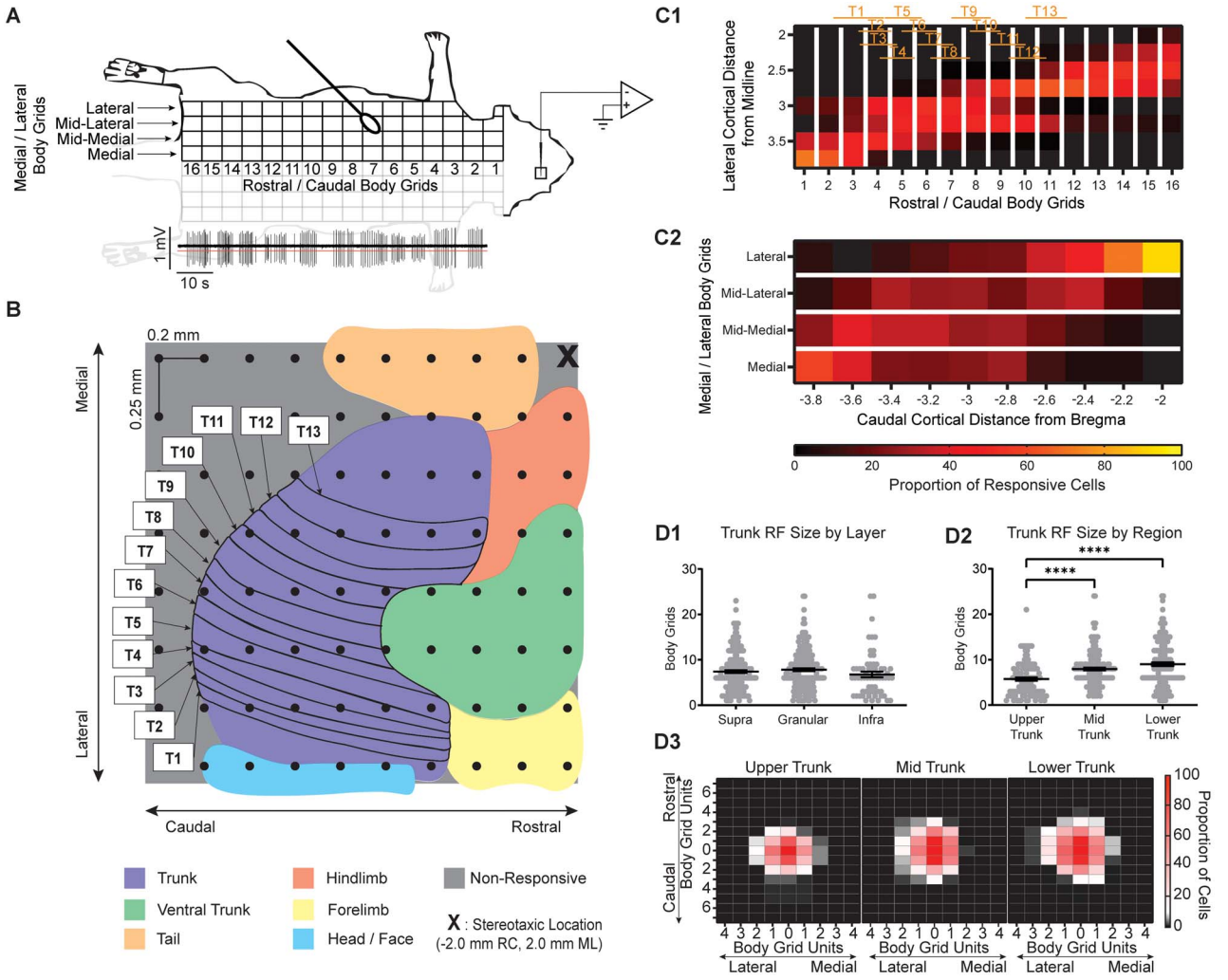

Figure 2. Relationship between trunk S1 organization and spinal dermatomes. (A) Sensory map methodological diagram. A tungsten microelectrode was inserted into several locations within and around trunk S1. Single units were isolated, and their receptive fields were determined. (B) Cortical representation of the thoracic dermatomes. The map shows the average cortical representations across cortical layers. Based on a pilot study ($N = 3$), 80 predefined cortical locations were chosen (black dots). They extended from −2.0 mm to −3.8 mm rostrocaudal (RC) from bregma with a resolution of 0.2 mm, and from −2.0 mm to −3.75 mm mediolateral (ML) with a resolution of 0.25 mm between locations, in order to optimally map the dorsal trunk area. Two thousand nine hundred and twenty neurons were recorded across all animals ($N = 40$) to construct the map. (C1) Proportion of cells identified in the mediolateral cortical axis across all animals, associated with body grid rows, to light tactile stimulation of which the cortical cells responded. A higher proportion of rostral trunk RFs were found at lateral cortical coordinates, whereas a higher proportion of caudal trunk RFs were found at medial cortical coordinates. The rostrocaudal extent of the thoracic dermatomes relative to the body grid rows are also displayed. (C2) Proportion of cells identified in the rostrocaudal axis across all animals, associated with body grid columns, to light tactile stimulation of which the cortical cells responded. A higher proportion of lateral trunk RFs were found at rostral cortical coordinates, whereas a higher proportion of medial trunk RFs were found at caudal cortical coordinates. The color scale bar at the bottom is for both (C1) and (C2). (D1) Trunk receptive field size (body grids units) ($N = 482$) of neurons in the supragranular, granular, and infragranular layers are similar. (D2) Receptive field size ($N = 437$) is significantly different for the upper, mid, and lower trunk S1 regions. (D3) Receptive field centers are normalized to position (0, 0) and the proportion of cells responsive to the surrounding body grids are calculated and showed significant differences in size across trunk S1 regions (refer to D2).

DV), and infragranular (1200 μm DV) cortex was selected for further analysis (Supplementary Fig. 3). For each layer, the SEP was considered responsive if the amplitude exceeded the mean background activity by 3 standard deviations (SDs). SEP amplitude was evaluated as the absolute value of the first negative peak of the SEP, normalized to the background activity. Peak latency of the SEPs was calculated as the time of the SEP peak amplitude post stimulus. Only responsive SEPs with a latency ≤50 ms were considered for further analysis to capture the short latency response. In addition, the LFP from each electrode was filtered (300–8000 Hz) and single neurons were discriminated using PCA and visual inspection using Offline Sorter (Plexon Inc., Dallas, TX, USA).

Single neuron spike times were used to construct peristimulus time histograms (PSTH) to determine the magnitude of the response of a neuron to the peripheral electric stimulation using previously published methods (Foffani and Moxon 2004; Tutunculer et al. 2006; Foffani et al. 2008; Kao et al. 2009; Manohar et al. 2017). The PSTH consisted of spike counts within 5 ms bins averaged across 100 trials within a window of 100 ms from the time of stimulus (Fig. 3E). A neuron was considered responsive if at least 2 consecutive bins in the PSTH exceeded 3 SDs above the

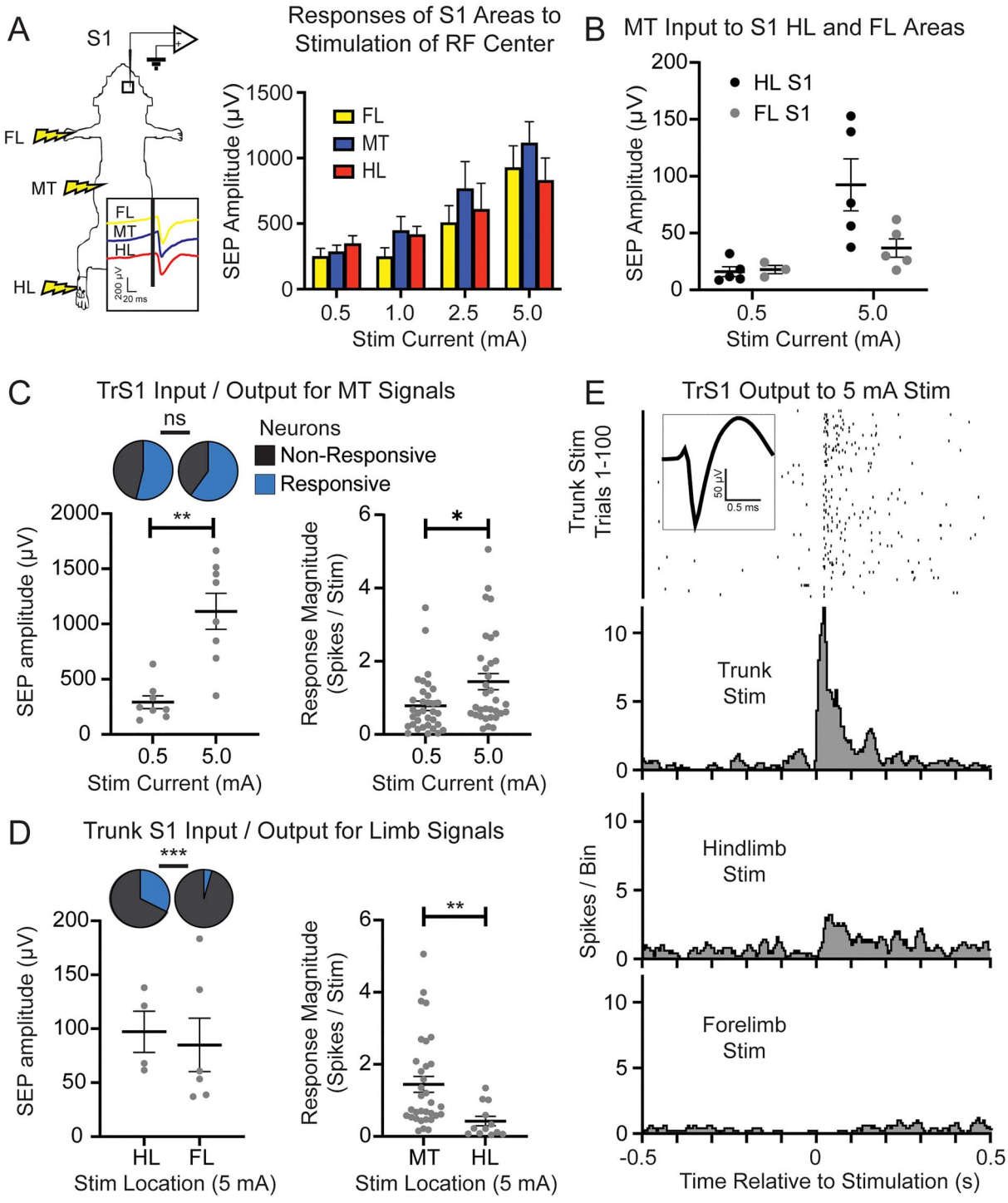

Figure 3. Somatosensory integration within trunk S1. (A) Electric stimulation methodological diagram. Multichannel recordings were performed in the trunk, forelimb, and hindlimb S1 in response to peripheral electrical stimulation to the mid trunk (MT), forelimb (FL), and hindlimb (HL). The SEP from each cortical region recorded from the granular layer to graded peripheral electric stimulation (0.5 mA, 1.0 mA, 2.5 mA, 5.0 mA) of each respective region (FL [$N = 5, 6, 7, 8$], HL [$N = 7, 6, 6, 7$], MT [$N = 9, 7, 6, 8$]) was compared (also see Supplementary Fig. 2). (B) SEP amplitude in the forelimb S1 and hindlimb S1 in response to the low intensity (0.5 mA; FLS1 [$N = 3$], HLS1 [$N = 5$]) and the high (5.0 mA; FLS1 [$N = 5$], HLS1 [$N = 5$]) MT stimulation. (C) The relationship between sensory inputs (SEP amplitude in the granular layer, left) (0.5 mA $N = 8$; 5.0 mA $N = 8$) and outputs (single neuron activity in all layers, right) (0.5 mA $N = 34$, 5.0 mA $N = 33$) in trunk S1 in response to low and high intensity MT stimuli. The inset on the top left represents the proportion of responsive cells for each stimulus. (D) Bottom left: SEP amplitudes recorded from trunk S1 in response to high intensity HL ($N = 4$) and FL ($N = 6$) stimulation. Top left: Proportion of trunk S1 neurons responding to hindlimb or forelimb stimulation. Right: Trunk S1 response to MT ($N = 33$) and HL ($N = 12$) stimulation calculated within 100 ms from stimulus onset. (E) Example PSTHs for trunk, HL, and FL stimulation (5.0 mA) in trunk S1, illustrating that trunk S1 activity is modulated more by hindlimb than forelimb.

background window. Response magnitude and the proportion of responsive neurons were quantified from neurons recorded across all layers in S1.

Mapping Trunk Motor Cortex

The representation of trunk primary motor cortex (TrM1) was examined by analyzing evoked movement and EMG activity in response to stimulation of infragranular neurons in M1 using previously published methods (Ganzer et al. 2016). Animals were anesthetized with ketamine (63 mg/kg, IP), xylazine (6 mg/kg, IP) and acepromazine (0.05 mg/kg, IP) and administered dexamethasone (5 mg/kg, IM) to control blood pressure and brain swelling. Supplemental doses of ketamine (20 mg/kg, IP) were administered when necessary, to maintain the animal at light Stage III-2 anesthesia throughout the entire mapping procedure (Friedberg et al. 1999; Tandon et al. 2008). Animals were placed in a stereotaxic frame in a prone position such that the limbs could hang freely. Eight bipolar intramuscular electromyogram (EMG) electrodes (stainless steel, 7 strands, AM-Systems Inc., Sequim, WA, USA) were implanted on dorsal (longissimus) and ventral (external oblique) trunk muscles at the upper thoracic (T4–T5), mid thoracic (T9–T10), and lower thoracic (T12–T13) levels. One EMG electrode was implanted in each of the contralateral shoulder/trunk (spinous trapezius [SP]), contralateral forelimb (forelimb bicep), contralateral hindlimb hip (gluteus maximus), and hindlimb ankle (tibialis anterior; Fig. 4A). Based on previous studies on rats (Neafsey et al. 1986; Oza and Giszter 2015; Ganzer et al. 2016), a craniotomy exposed the medial post bregma area and the caudal forelimb area (1 mm to −3.5 mm RC, 1–3 mm ML). Similar to the somatosensory mapping procedure, 88 predefined cortical locations were chosen spanning the craniotomy. The medial portion (<1 mm) could not be mapped reliably due to methodological constraints related to the high density of blood vessels in this region that limits access to the cortex. Previously, (Donoghue and Wise 1982) reported that responses could not be evoked from these medial regions. This region, often referred to as medial agranular cortex or M2, is cytoarchitecturally different from M1.

A low impedance glass insulated tungsten electrode (100–500 kΩ; FHC Inc., Bowdoin, ME, USA) attached to a stereotaxic manipulator was inserted into one of the 88 predefined cortical locations. In order to assess microstimulation waveform quality, the voltage drop across a 10 kΩ resistor interposed in series between animal ground and the isolated current pulse stimulator (Model 2100, A-M systems, Sequim, WA, USA) was monitored with an oscilloscope. At each M1 location, the electrode was lowered to the infragranular layer (1.5 mm DV) and a long-train ICMS was applied (Young et al. 2011; Griffin et al. 2014), consisting of 0.2 ms cathodal leading bipolar current pulses (10–100 µA) delivered at 333 Hz for 300 ms. This long train was used to evoke muscle synergies (overlapping representations/coactivation of segmental muscle groups) that represent complex movement repertoires. Pilot experiments with 60 ms stimulus trains showed that stimulus-evoked movement represented short, truncated movements and muscle twitches. Although 300 ms pulse trains often elicited a variety of movements ranging from simple (muscle contraction across a single joint) to more complex movements that represented the coactivation of muscles across different segmental levels of trunk/across multiple joints consistent with other studies (Graziano et al. 2002; Ramanathan et al. 2006; Giszter et al. 2008; Brown and Teskey 2014; Overduin et al. 2014; Baldwin et al. 2017; Halley et al. 2020). The stimulation current was gradually increased in steps of 10 µA until a reliable movement or EMG response was found.

EMG signals and current stimulus times were sent to a data acquisition system (Intan Technologies, Los Angeles, CA, USA). EMG was sampled at 5 kHz, zero-lag band pass filtered (40–400 Hz) and rectified. An EMG envelope was obtained by further filtering the data (zero-lag Butterworth low pass filter, 20 Hz, fifth order). The EMG envelope was normalized to its peak value to account for changes in EMG response due to electrode placement, impedance mismatch, signal to noise ratio, and muscle size (Kargo and Nitz 2003). Motor evoked potentials (MEPs) were then obtained by averaging the processed EMG over a time window of 1 s centered on the current stimulus timestamps. If the amplitude of a MEP exceeded the background EMG activity by 5 SD, it was considered a responsive EMG. The minimum current required for eliciting a movement/EMG response was defined as the threshold current for that cortical location. Once a reliable threshold current was found, the current was increased to 100 µA (suprathreshold), and the movement and EMG responses were recorded. A minimum of 5 separate stimulations were performed in every cortical location. If no movement or EMG response was evoked with the 100 µA current, the cortical location was determined nonresponsive. If there were more than 3 consecutive nonresponsive locations, the closest responsive location was rechecked to identify the limits of motor cortex. A combination of visual observation of movements and responsive EMG locations were used to classify cortical locations into movement types (Table 1). Recruitment of trunk musculature via stimulation of the TrM1 was examined based on EMG response. Trunk musculature responses were classified into different categories based on the location of responsive trunk EMG along the thoracic level at both threshold and suprathreshold currents (Table 2, Fig. 5A). At threshold, the proportion of responsive EMG was compared across thoracic levels.

The muscle responses (muscle identification and movement type) associated with the stimulation of each cortical location were used to calculate a responsiveness score (Girgis et al. 2007; Ganzer et al. 2016). For each movement type (or trunk musculature type), the proportion of responses in each location was determined and transformed to a score as follows: ranges of 0, 1–33%, 34–66%, and 67–100% received a score of 0, 1, 2, or 3, respectively. For example, if only 1 animal responded to cortical stimulation at a cortical location out of 5 animals that were stimulated at that spot, the occurrence rate would be 0.2 or a score of 1. A score of 0 meant that no movement and no EMG response were recorded and a score of 3 meant that the muscle movement (or EMG response) was elicited for 67–100% of the cortical stimulation. The average responsiveness score for a specific movement type and/or EMG response was calculated by averaging the score across cortical locations. To control for the fact that not every cortical location was sampled equally, a responsiveness score was only included in the analysis if there were at least 5 penetrations in a given location.

Retrograde Tracing

To gain insight into the regions of the brain that project sensory input to TrM1, a tracing study was performed. Results from the ICMS mapping showed that only a small location in the brain exclusively activated trunk musculature and most of TrM1 included coactivation with other body parts. However, the location of this exclusively trunk area was variable across

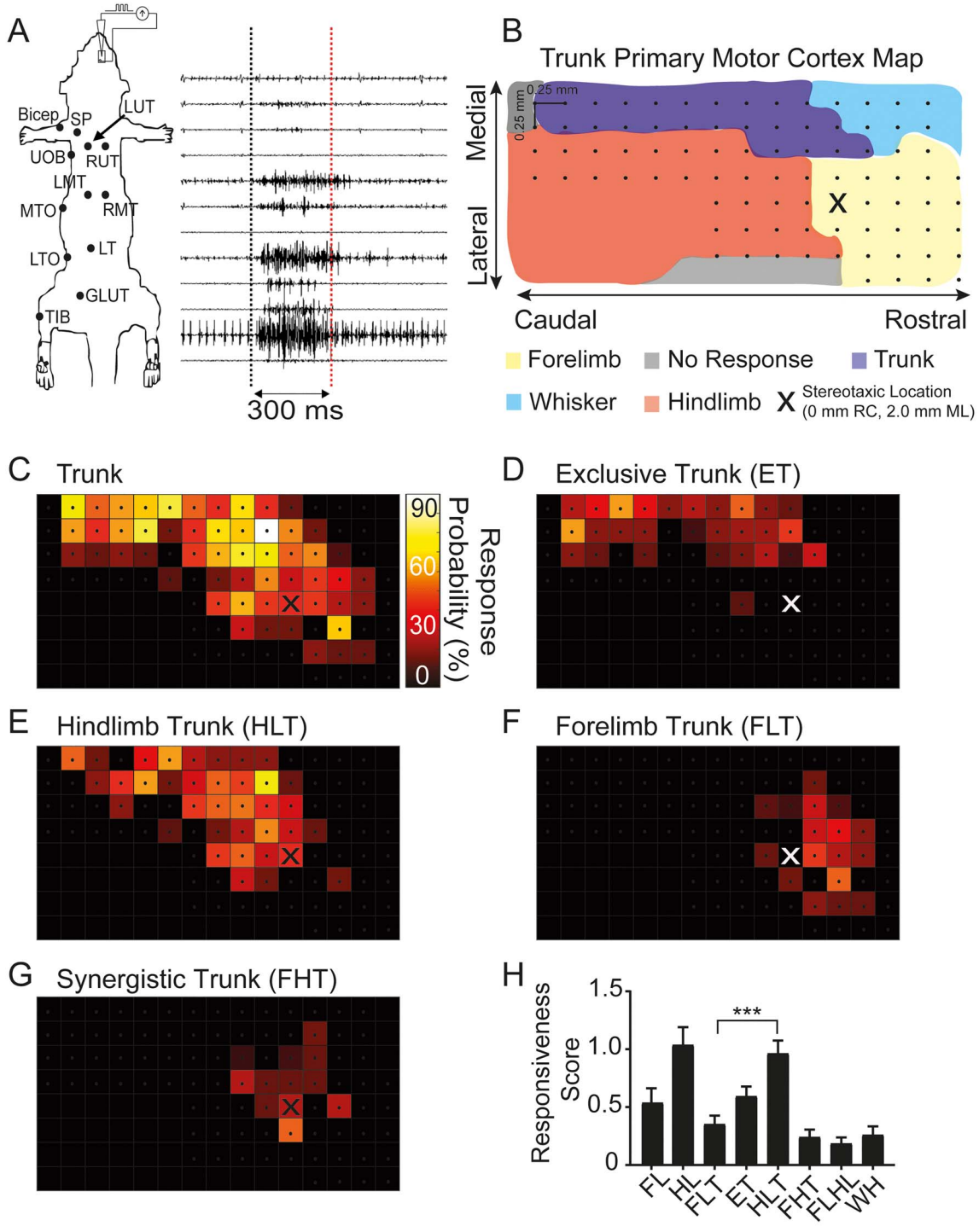

Figure 4. Coactivation of trunk musculature with forelimb and hindlimb. (A) ICMS methodological diagram. Motor maps were obtained by intracortical current microsimulation (ICMS) in the infragranular layer of motor cortex. Evoked muscle activity was recorded through EMG electrodes implanted along the trunk, forelimb, and hindlimb musculature (top to bottom: forelimb bicep [bicep], spinous trapezius [SP], left upper thoracic longissimus [LUT], right upper thoracic longissimus [RUT], upper external oblique [UOB], left mid thoracic longissimus [LMT], right mid thoracic longissimus [RMT], mid thoracic external oblique [MTO], lower thoracic longissimus [LT], lower thoracic external oblique [LTO], gluteus maximus [Glut], tibialis anterior [Tib]). Observed movement and evoked muscle activity at threshold current were used to determine movement representation. (B) Topography of TrM1 is based on the most predominant response across animals. The dots refer to penetration locations sampled across animals. The X location refers to 0 mm RC, 2 mm ML, relative to bregma. (C–G) Proportion of penetrations from which the following muscles were activated: (C) trunk, (D) trunk exclusively, (E) trunk and hindlimb, (F) trunk and forelimb, and (G) trunk and both forelimbs and hindlimbs. (H) Average responsiveness score within trunk M1 ($N = 54$) was calculated for the different movement representations identified during mapping with ICMS (see Materials and Methods for explanation). FL (activation of forelimb only), HL (activation of hindlimb only), FLT (coactivation of only forelimb and trunk), ET (exclusively trunk or activation of only trunk), HLT (coactivation of only hindlimb and trunk), FHT (coactivation of forelimb, hindlimb and trunk), FLHL (coactivation of only forelimb and hindlimb), WH (activation of whisker pad).

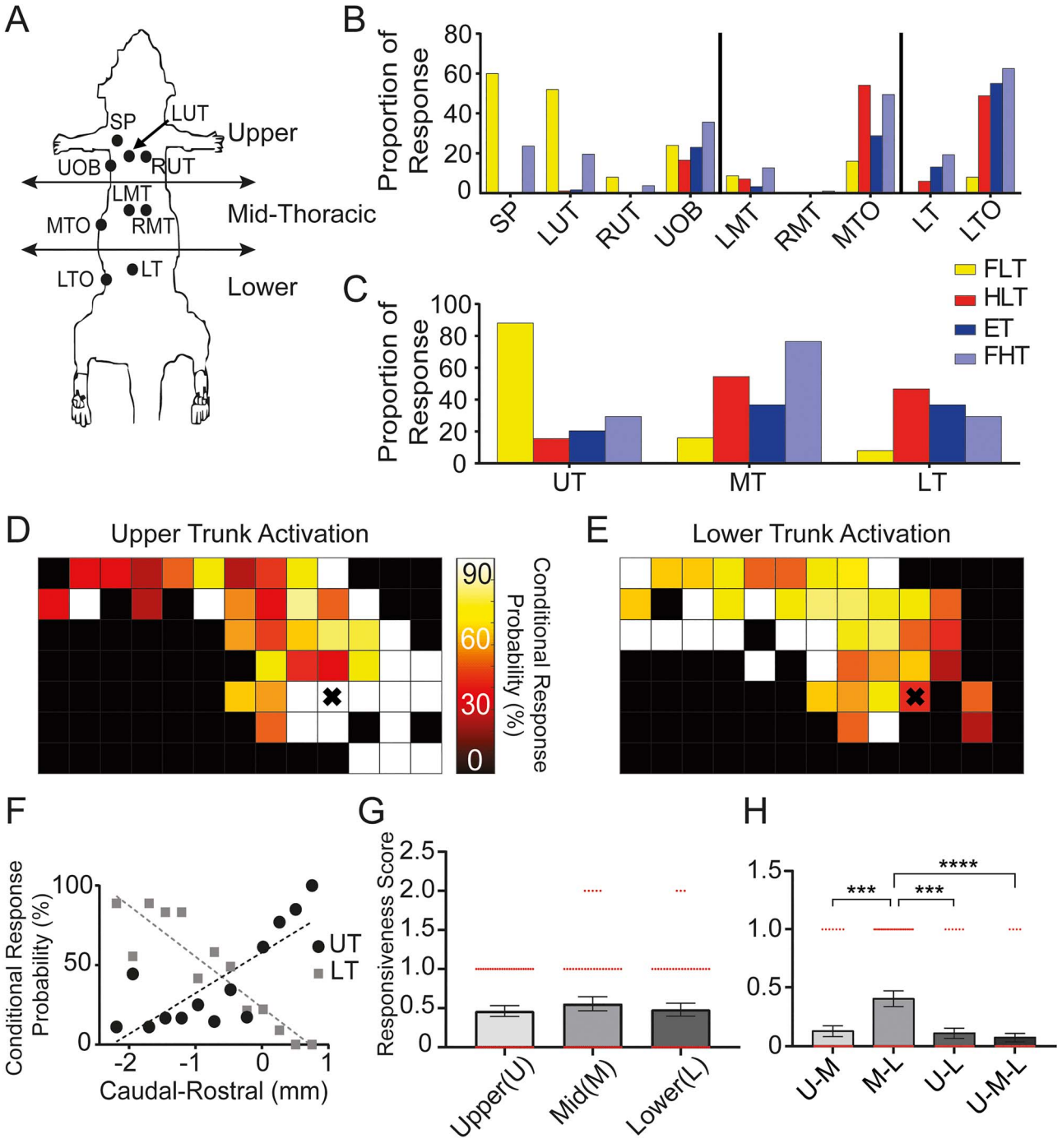

Figure 5. Recruitment of trunk musculature in the different coactivation zones. (A) Methodological diagram showing EMG electrode locations of trunk muscles categorized into three groups along the rostrocaudal axis of the body: upper thoracic, mid thoracic, and lower thoracic trunk muscles. (B) Proportion of muscle responses in the different coactivation zones by muscle. (C) Same graph as B, but muscles are grouped within the three segmental zones seen in (A). Upper thoracic muscles were activated when FLT coactivation zone was stimulated and lower thoracic muscles were activated when HLT coactivation zone was stimulated. (D–E) For locations within TrM1, the conditional probability of activating upper trunk musculature (D) is compared to activating lower trunk musculature (E). The X location refers to 0 mm RC, 2 mm ML, relative to bregma. (F) Graph showing the conditional probability of eliciting trunk muscle responses in TrM1 based on visual observation & EMG responses of either upper or lower trunk musculature averaged across the rostrocaudal axis. (G) Average responsiveness score within TrM1 (see Materials and Methods; $N = 54$) for the different segmental zones: upper, mid, and lower thoracic. (H) Differences in the likelihood of segmental coactivation were also plotted within TrM1 for each of the segmental coactivations.

Table 1 Movement type classification

Movement type	Visual observation	EMG response
Forelimb (FL)	Isolated movement of forelimb (wrist or multijoint)	Exclusive EMG response—FL muscle (FL bicep)
Hindlimb (HL)	Isolated movement of hindlimb (digits or multijoint)	Exclusive EMG response—HL muscles (gluteus, tibialis)
Forelimb trunk (FLT)	Proximal shoulder movement	Coactivation of FL muscle and Trunk/shoulder muscles
Exclusively trunk (ET)	Isolated movement of thoracic girdle	Exclusive EMG response—trunk muscles
Hindlimb trunk (HLT)	Movement of hindlimb knee/ankle along with thoracic girdle	EMG response—trunk muscles
Synergistic trunk (FHT)	Forepaw and HL ankle dorsiflexion movements with trunk adduction	EMG response—Trunk muscles
Forelimb–Hindlimb (FLHL)	Exclusive forepaw and HL ankle dorsiflexion movements	Coactivation of forelimb and hindlimb muscles
Whisker (WH)	Whisker movements	Absence of any EMG response

Note: Explanation of how movement types were determined for each intracortical microstimulation trial.

Table 2 Trunk musculature classification

Trunk musculature type	EMG response
Dorsal trunk	Activation of spinous trapezius or longissimus muscles at upper, mid, or lower thoracic level
Ventral trunk	Activation of external oblique muscles at upper, mid, or lower thoracic level
Upper thoracic trunk (U)	Activation of spinous trapezius (SP), left upper thoracic longissimus (LUT), right upper thoracic longissimus (RUT), or upper external oblique (UOB)
Mid thoracic trunk (M)	Activation of left mid thoracic longissimus (LMT), right mid thoracic longissimus (RMT), or mid thoracic external oblique (MTO)
Lower thoracic trunk (L)	Activation of lower thoracic oblique (LTO) or lower thoracic longissimus (LT)

Note: Muscles that were activated in response to intracortical microstimulation were classified as one of five muscle types.

animals. Although an ICMS study prior to tracer injection could have located this exclusively trunk region in each animal, this would have severely damaged the tissue and made the tracing unreliable. Therefore, the tracer was injected into the most likely location that exclusively activated trunk musculature. Animals were anesthetized with ketamine (63 mg/kg, IP), xylazine (6 mg/kg, IP), and acepromazine (0.05 mg/kg, IP). A craniotomy was made over TrM1 (−0.5 mm RC, 1.25 mm ML, 1.65 mm DV) and 300 nL of 10% fluorescent microbeads (Lumafluor Inc., Naples, FL.; Figs. 4D and 7A) were injected with a Hamilton syringe (tip diameter: 0.1 mm). Three days after the injection, animals were perfused with saline followed by 4% PFA and brains were removed. Fifty microliters coronal sections were mounted under Permount (Fischer Chemical, Geel, Belgium) on microscope slides. Brain slices were then imaged using a wide field microscope (5×/.012 numerical aperture; ZEISS, Oberkochen, Germany) and cell counting was performed using ImageJ (National Institutes of Health, Bethesda, MD, USA). Images were transformed to an 8-bit gray scale image and thresholding was done to minimize artifacts caused by autofluorescence. Automated cell counting (minimum size: 100 pixels^2) was conducted in the region of interest (ROI). The different ROIs, corresponding to the different somatosensory cortices were identified based on electrophysiological sensory mapping data (Fig. 2B). For locations outside of TrS1, ROIs for HLS1 and FLS1 were identified based on (Leergaard et al. 2004). Only ipsilateral projections were identified. The location of thalamic nuclei was identified by superimposing our images on to the rat brain atlas (Paxinos & Watson 2007).

Postural Control Task (Tilt Task)

The tilt task was used to understand sensorimotor integration in the cortex relevant for postural control. Microwire arrays (32 channel each [8×4], 250 µm resolution, Microprobes, Gaithersburg, MD, USA) were implanted bilaterally in the infragranular layer of the cortex, spanning TrS1, HLS1, and FLS1 on the left hemisphere and TrM1 and on the right hemisphere. For chronic microwire implantation refer to previously published methods (Foffani et al. 2008; Manohar et al. 2012; Bridges et al. 2018). Single neuron activity was recorded from the different cortices in response to sudden unexpected postural perturbation in the lateral plane. Four different tilt types were tested, two to the left and two to the right. For each direction, there was a slow speed (max speed: 26.2°/s; duration to final amplitude: 0.9 s) and a fast speed (max speed: 76.5°/s; duration to final amplitude: 0.5 s). The final angle for all tilt types had the same final amplitude of 16.5° (Fig. 8A). The task was adapted from (Bridges et al. 2018) and engaged the cortex bilaterally. Based on the mapping results, the recording electrodes in M1 were grouped based on the region of the body they most likely activated. Electrodes spanning caudal TrM1 (−1 mm to −2 mm RC, 1.25–1.5 mm ML; Fig. 5F) preferentially activated lower thoracic trunk musculature and were defined as lower thoracic trunk primary motor cortex (LTM1). Electrodes rostral to LTM1 (0 mm to −0.75 mm RC, 1.25–2.0 mm ML) were more likely to control upper thoracic muscles and were labeled upper trunk primary motor cortex (UTM1). Regions lateral to LTM1 (−1 mm to −2 mm RC, 1.75–2 mm ML) preferentially controlled hindlimb musculature (HLT) and were defined as hindlimb primary motor cortex (HLM1). Similarly,

for each of the electrodes spanning the somatosensory cortex (left hemisphere), the corresponding RF center (i.e., stimulus location that produced the largest SEP amplitude) was identified in response to peripheral electric stimulation (0.5 mA, tactile) of the different body parts (forelimb, hindlimb, upper, mid, and lower trunk). The electrode was then labeled as recording from FLS1, HLS1, UTS1, MTS1, or LTS1 based on the RF center.

Responsiveness in the different cortices was calculated as the proportion of responsive neurons to at least one tilt type. A neuron was considered responsive to a tilt if the neuronal activity in the response window (400 ms from start of tilt) was significantly different from the background and there were at least 5 consecutive bins (bin size 5 ms) in the response window that exceed the background activity by 2 SD. The magnitude of response (spikes per second) was defined as the change in the average neuronal firing rate from the background (average firing rate in response window—average background firing rate). Shannon's mutual information was used to quantify the information about the tilt type provided by the neuronal response of each single neuron within the region (Liu et al. 2017). If a neuronal response and a tilt type are completely independent from each other, mutual information is 0 bits, and if they are perfectly correlated, the mutual information is defined by the entropy of the stimulus (tilt type) and is 2.0 bits (i.e., $\log_2(4)$, $n = 4$ tilt types) of information.

Statistical Analysis

Statistical analyses were conducted using GraphPad Prism 9.0.1. Continuous variables with a normal distribution are reported as mean + standard error; variables with a non-normal distribution are reported as median (interquartile range). Differences between 2 independent groups were assessed using an Independent Samples *t*-test for normally distributed data, or a Mann–Whitney *U* test for non-normal data. Differences between three or more independent groups were assessed using analysis of variance (ANOVA) with a Tukey post hoc test for normally distributed data, or a Kruskal–Wallis test with a Dunn's post hoc test for non-normal data. Frequencies were compared using Pearson χ^2 or Fisher's exact test. A value of $P < 0.05$ was considered significant and significant group effects were subjected to Tukey's honest significant difference post hoc test. $P < 0.05$ is denoted by *, $P < 0.01$ by **, $P < 0.001$ by ***, and $P < 0.0001$ by ****.

Results

Dermatomes of Upper Thoracic DRGs Overlap More than those of Lower Thoracic DRGs

To study how trunk somatosensory information is represented in the brain, it is important to understand how this somatosensory information is first represented at the spinal level. Although the upper and lower thoracic dermatomes were previously mapped (Lombard et al. 1979; Smith 1986; Takahashi et al. 1994; Wessels et al. 1994), the mid thoracic dermatomes have not been mapped extensively in the rat, nor is the representation of these dermatomes in the cortex known. To this end, we recorded single neuron activity from DRGs at the thoracic level (T1–T13) and mapped the thoracic dermatomes (Fig. 1A). An average of 6 ± 3 DRGs were recorded per animal ($n = 15$) for a total of 86 recorded dermatomes. The thoracic dermatomes were rectangular bands with overlapping RFs that extended from the dorsal midline to the midline on the ventral side of the trunk. The T1–T3 dermatomes had RFs that extended into the forelimb, whereas the RFs of the remaining thoracic dermatomes were limited to the trunk (Fig. 1B). The width of the thoracic dermatomes remained constant in the RC direction along the body (One-way Repeated Measures ANOVA, F (12, 59) = 1.41, $P = 0.44$; Fig. 1C), consistent with studies performed on cats (Kuhn 1953; Hekmatpanah 1961), sheep (Kirk 1968), and monkeys (Sherrington 1892; Kirk and Denny-Brown 1970). However, the amount of overlap between adjacent dermatomes decreased significantly from rostral to caudal (One-way Repeated Measures ANOVA, F [11, 44] = 2.52, $P < 0.05$; Fig. 1D). This decrease in overlap was due to a shift in the average center position of adjacent dermatomes (One-way ANOVA, F [2, 61] = 7.73, $P < 0.001$; Fig. 1E). Tukey's post hoc test revealed a significant increase in the average positional shift distance between adjacent dermatomes in both the mid (T5–T9; $P < 0.05$) and lower (T9–T13; $P < 0.001$) trunk regions when compared to upper trunk dermatomes (T1–T5). Therefore, rostral DRGs appeared to overlap more with neighboring dermatomes than caudal DRGs.

Sensory Information from Mid and Lower Trunk most Likely to Overlap within S1

A somatotopic map of TrS1 and surrounding somatosensory cortices was constructed using single unit cortical mapping data as well as information from the dermatomes. In each cortical location, the proportion of cells responding to each body part was calculated (Fig. 2A). An average of 9 ± 3 cortical locations were sampled per animal ($N = 40$ animals), with an average of 8 ± 3 single neurons sampled per location. In total, more than 2900 neurons were recorded. TrS1 was determined to be located along the caudal edge of FLS1 and HLS1, consistent with previous studies in rats (Chapin and Lin 1984; Xerri et al. 1994; Seelke et al. 2012). The representation of the neck was most lateral, with the tail representation most medial (Fig. 2B). Dorsal TrS1 was located more caudal to ventral TrS1. The ventral TrS1, consistent with previous studies (Chapin and Lin 1984; Xerri et al. 1994; Seelke et al. 2012), was nestled between the FLS1 (lateral) and the HLS1 (medial), and rostral to mid thoracic (T6–T9) trunk representations, overlapping with the genital cortex described in previous studies (Lenschow and Brecht 2018). The full rostral extent of ventral trunk was not mapped. Nonetheless, these results show that the trunk representation is larger than previously reported (Hall and Lindholm 1974; Gioanni and Lamarche 1985; Ganzer et al. 2016).

Within the trunk representation, the thoracic dermatomes were represented from T1, laterally, to T13, medially, consistent with a study in humans (Itomi et al. 2000). As might be expected, there was extensive overlap of the cortical representation of neighboring thoracic dermatomes (Fig. 2C). The RC dimension of the dorsal trunk body was represented along the ML axis of the cortex, with rostral trunk body represented laterally in the TrS1 (Fig. 2 C1). The ML dimension of the dorsal trunk body was represented along the RC axis of the cortex, with the most lateral part of dorsal trunk body represented rostrally in the cortex, just caudal to the ventral trunk representation (Fig. 2C2). Unlike other sensory systems, such as whisker and limbs that tend to have RF size differences across layers (Chapin 1986), the RF size of neurons in TrS1 were similar across layers ($N = 482$) (One-way ANOVA, F [2, 479] = 1.45, $P = 0.23$; Fig. 2 D1). However, the RF size of trunk neurons did differ across the different

regions of the TrS1 ($N = 437$) (One-way ANOVA, F [2, 434] = 19.71, $P < 0.0001$; Fig. 2D2) with upper trunk neurons having smaller RF size compared to both mid and lower trunk neurons (5.7 ± 3.7, 8.0 ± 3.8, 9.0 ± 5.0 body grids or cm^2, respectively; Tukey's post hoc test, $P < 0.0001$; Fig. 2D2–D3). This RF size analysis suggests that somatosensory information ascending from the thalamus is spread across large parts of TrS1 early, immediately upon arrival in layer IV, with more overlap between mid and lower trunk sensory information than that of upper trunk. This is consistent with RF sizes observed in forepaw somatosensory cortex that varied from relatively small in the digits to larger in the limb (Foffani et al. 2008).

Greater Overlap of Trunk S1 with Hindlimb than Forelimb S1

To understand the overlap between trunk, forelimb, and hindlimb somatosensory information, multichannel recordings were performed in TrS1, FLS1, and HLS1 in response to peripheral electrical stimulation of the mid trunk, forelimb, and hindlimb. To ensure fair comparison between the responses to the different stimulus locations on the body, the amplitudes of the SEP recorded from the granular layer at each cortical region in response to graded peripheral electric stimulation of each respective region (FL, HL, and MT) were compared (Fig. 3A, Supplementary Fig. 2B). As expected, there was a significant increase in the SEP amplitude associated with increases in stimulus current regardless of stimulus location (Two-way Repeated Measures ANOVA, F [3, 70] = 15.47, $P < 0.0001$; Fig. 3A). However, across stimulus location, the SEP amplitudes were similar (Two-way Repeated Measures ANOVA, F [2, 70] = 1.62, $P = 0.21$; Fig. 3A), suggesting that the stimulus at each location activated the homologous cortical region similarly and that comparisons could be made between responses recorded from different brain regions to stimulation of the same location on the body.

To understand the overlap of trunk somatosensory information across S1, the amplitude of the SEP response to mid trunk stimulation recorded from FLS1 was compared to the SEP response recorded from HLS1. The SEP amplitudes recorded from FLS1 and HLS1 in response to low intensity trunk stimulation (0.5 mA) were similar (Independent Samples t-test, t [6] = 0.29, $P = 0.77$), suggesting trunk somatosensory information overlaps with both FLS1 and HLS1. However, when the stimulation amplitude was increased to produce twitching of the underlying muscle and further activate proprioceptive receptors (5.0 mA), the response in HLS1 was significantly greater than that recorded from FLS1 (Independent Samples t-test, t [8] = 2.30, $P = 0.05$; Fig. 3B, Supplementary Fig. 2C–D), suggesting differences in the overlap of trunk somatosensory information in HLS1 compared to FLS1.

Next, within TrS1, the relationship between inputs to layer IV cells (SEP amplitude) and outputs of TrS1 neurons (single neuron firing rate or proportion of responding neurons) in response to low and high intensity mid trunk stimuli were examined to assess the effectiveness of the information transfer from input to output (Fig. 3C). As noted above, SEP amplitude to high intensity mid trunk stimulation was significantly greater than the response to low-intensity stimulation (Independent Samples t-test, t [14] = 4.76, $P < 0.001$). This increase in input results in a greater magnitude of the response (spikes per stimulus) to high-intensity stimuli (Independent Samples t-test, t [65] = 2.59, $P < 0.05$; Fig. 3C) without a change in the proportion of responsive neurons (χ^2 [1, $N = 55$] = 0.46, $P = 0.50$), suggesting the same cells are responding to low-intensity stimuli as those that respond to high intensity.

Next, the contribution of high intensity forelimb and hindlimb stimulation to the response in TrS1 was examined. The SEP amplitude in TrS1 to forelimb stimulation was similar to that of hindlimb stimulation (Independent Samples t-test, t [8] = 0.36, $P = 0.73$). However, the proportion of neurons in TrS1 that responded to hindlimb stimulation was greater than the proportion responding to forelimb stimulation (χ^2 [1, $N = 84$] = 11.16, $P < 0.001$; Fig. 3D), suggesting that the transfer of incoming somatosensory information to output is more effective for hindlimb than forelimb stimulation. In fact, too few cells responded to forelimb stimulation to allow any further analysis.

To understand if the increased proportion of responsive TrS1 cells to hindlimb stimulation was potentially influenced by the proximity of these body or somatotopic regions, recordings were performed in upper TrS1 during stimulation to forelimb and hindlimb (5.0 mA; $n = 3$). No differences were found in SEP amplitude (Independent Samples t-test, t [4] = 0.09, $P = 0.92$) or the proportion of responsive cells (χ^2 [1, $N = 107$] = 2.95, $P = 0.09$) between stimuli conditions, suggesting that proximity is likely not contributing to increased responsiveness (Supplementary Fig. 2E).

As expected, the response of TrS1 neurons to hindlimb stimulation was smaller than the response to MT stimulation (Independent Samples t-test, t [43] = 2.71, $P < 0.01$; Fig. 3D and E). These results, taken together, suggest reciprocal flow of information between TrS1 and both FLS1 and HLS1, with greater influence of trunk somatosensory information in HLS1 compared to FLS1 and greater influence of hindlimb somatosensory information in TrS1 compared to forelimb information. In the last section of this paper, we explore how this organization is used to encode the cortical response to unexpected tilts in the lateral plane.

Coactivation of Trunk Musculature with Hindlimb Is more Likely than Coactivation with Forelimb Musculature

To gain a better understanding of the trunk cortex, it was essential to examine the extent and organization within TrM1. The extent of TrM1 was mapped using ICMS and movement representations were examined by analyzing movement and EMG responses from trunk and limb musculature (Fig. 4A). Each of the 88 cortical locations were sampled an average of 7 ± 2 times, across 21 animals. Each animal contributed to the data with an average of 27 ± 2 cortical locations per animal. The average threshold current was 51.3 ± 23.4 mA. The areas of the cortex that most likely activated the trunk musculature were within 1.5 mm ML and 0.25 mm to −2.25 mm RC, relative to bregma (Fig. 4B). This placed the rat TrM1 medial to FLM1 and HLM1 and just caudal to whisker M1.

A much larger area than previously reported activated trunk by generally coactivating with other parts of the body, suggesting that this coactivation with forelimb and hindlimb motor cortex is functionally relevant. For each animal, the area that exclusively activated trunk musculature (ET) was quite small, and the location of ET was not consistent across animals. This suggests that there are likely to be few conditions under which trunk musculature is activated independently of the musculature of other parts of the body. In fact, it is possible to identify distinct

coactivation zones between trunk and other parts of the body. The overall extent of the trunk coactivating with other parts of the body (Fig. 4C) spanned −2.25 mm to 0.75 mm RC and 1–2.5 mm ML relative to bregma, which is much larger than previously reported (Gioanni and Lamarche 1985; Neafsey et al. 1986; Tandon et al. 2013; Frost et al. 2015; Oza and Giszter 2015; Ganzer et al. 2016). The area that exclusively activated trunk musculature (ET) within any given animal was restricted to within 1.5 mm lateral to midline (Fig. 4D).

Despite this small area devoted to ET, coactivation of trunk with HLT was quite large (Fig. 4E) and, not surprisingly, caudal to locations overlapping with forelimb musculature (FLT; Fig. 4F). In addition, consistent with an earlier study (Boyeson et al. 1991), in approximately half of the animals (45%), FL, HL, and trunk (synergistic trunk or FHT) coactivated in locations between the HLT and FLT representation (Fig. 4G). In order to quantify and compare the different movement representations found within the trunk coactivation zone, responsiveness scores (Girgis et al. 2007; Ganzer et al. 2016) that represented the proportion of responses for each representation were compared. The responsiveness scores were different across coactivation zones ($N = 54$) (One-way ANOVA, F [7, 424] = 11.10, $P < 0.001$; Fig. 4H). Importantly, the responsiveness score of HLT was significantly greater than FLT (Tukey's post hoc test, $P < 0.01$), indicating that trunk coactivates more with hindlimbs across a larger region of cortex compared to forelimbs. Moreover, the responsiveness score of FLHL and FHT were very similar, suggesting that when forelimb and hindlimb coactivate, about half the time they coactivate with trunk. These results demonstrate that a large region of M1 is devoted to coactivating trunk musculature with musculature from different body parts, mainly hindlimb and less so with forelimb (Table 1).

Trunk Motor Cortex Is Somatotopically Organized

To understand trunk musculature recruitment associated with the different coactivation zones, EMG responses were examined in more detail. As expected, stimulation of forelimb trunk cortex (FLT) preferentially activated SP and contralateral upper thoracic longissimus (LUT). FLT coactivation zone is thus responsible for upper thoracic trunk muscles activation (Fig. 5A–C). Similarly, stimulation of hindlimb trunk cortex (HLT) activated the obliques along the mid and lower thoracic level and therefore HLT coactivation zone is preferentially responsible for mid and lower trunk muscles activation (Fig. 5A–C). Interestingly, stimulation of ET cortex also activated the oblique but at all thoracic levels, suggesting that ET is important to coordinate movements of the entire trunk. Finally, stimulation of the synergistic trunk cortex (FHT) activated mostly trunk musculature at the mid thoracic level (Fig. 5C). Therefore, the different trunk coactivation zones differentially activate segmental trunk muscles (upper, mid, and lower thoracic levels) providing topography to TrM1 motor control.

To gain more insight, we constructed 2 maps of trunk coactivation zone: the first to identify the proportion of penetrations across animals that activated upper trunk muscles (Fig. 5D) and the second to identify the proportion that activated lower trunk muscles (Fig. 5E). The mediocaudal region of trunk coactivation zone preferentially controlled lower thoracic trunk musculature whereas the rostrolateral region controlled upper thoracic trunk musculature. The lower trunk musculature was more influenced by the rostrolateral area of trunk coactivation zone and upper trunk musculature by the mediocaudal area of trunk coactivation zone. To demonstrate this topography along the RC axis, the proportion of penetrations activating upper or lower thoracic trunk from ML locations were averaged (Fig. 5F). Moving rostral, there was an increase in the probability of activating upper trunk (linear regression, $r^2 = 0.61$, F [1, 11] = 17.82, $P < 0.01$), whereas moving caudal, there was an increase in the probability of activating lower trunk (linear regression, $r^2 = 0.83$, F [1, 11] = 54.70, $P < 0.01$). This demonstrates a clear somatotopy within the trunk coactivation zone that define subregions of TrM1: UTM1 and LTM1.

Considering that segmental trunk muscles were differentially activated within this trunk coactivation zone, the amount and extent of activation within the coactivation zone was examined using the responsiveness score. The responsiveness scores were similar across the mid, upper, and lower thoracic segmental levels ($N = 54$, each level) (One-way ANOVA, F [2, 159] = 0.49, $P = 0.54$; Fig. 5G), suggesting that the probability of cortex to activate the different segmental levels exclusively is similar. However, despite this similarity, there were differences in the likelihood of segmental coactivation (One-way ANOVA, F [3, 212] = 9.06, $P < 0.001$; Fig. 5H) with the mid and lower thoracic muscles more likely to coactivate than other segmental muscle groups (Tukey's post hoc test, $P < 0.001$). In summary, most of TrM1 is devoted to activation with other regions of the body and cortical representation of mid and lower thoracic trunk muscles are associated with hindlimb muscle representation whereas upper thoracic trunk muscles are associated with forelimb muscle representation. These results were confirmed by synergy analysis using the amplitude of evoked EMG responses obtained from the different trunk musculature (Supplementary Fig. 1, Table 2).

Somatosensory Input to Trunk Motor Cortex Is Dominated by Hindlimb Information

Given our understanding of somatosensory overlap within S1 and coactivation of trunk muscles with other regions of the body, we examined the integration of TrM1 with somatosensory input from the limbs by recording neural response in TrM1 supragranular and infragranular layers in response to electric stimulation of forelimbs, hindlimbs, mid trunk or upper trunk (Fig. 6A). There was little to no response in TrM1 to low-intensity stimulation (0.5 mA) applied to any of the 4 body locations. However, this was not the case for high-intensity stimulation (5.0 mA). Surprisingly, the SEP amplitude recorded from TrM1 in response to high intensity somatosensory stimulation of the hindlimbs was greater than the SEP amplitude to stimulation of either mid or upper trunk (Fig. 6B and C). The response to forelimb stimulation was similar to that of trunk stimulation, solidifying that TrM1 preferentially receives somatosensory information from hindlimbs.

Due to the internal motor somatotopy along the RC axis of TrM1 (refer to Fig. 5F), cortical locations where SEPs were recorded were segregated into rostral (0 to −0.75 mm RC) and caudal regions (−1 to −2 mm RC). In the supragranular layer (Caudal, $N = 103$; Rostral $N = 96$), there was no effect of recording location (Two-way ANOVA, F [1, 191] = 2.34, $P = 0.13$), but there was an effect of stimulus location (Two-way ANOVA, F [3, 191] = 22.25, $P < 0.0001$; Fig. 6D) such that the SEP amplitude recorded from both rostral and caudal TrM1 in response to hindlimb stimulation was greater than the response to stimulation of all the other locations (Tukey's post hoc test, $P < 0.0001$). This result demonstrates an important

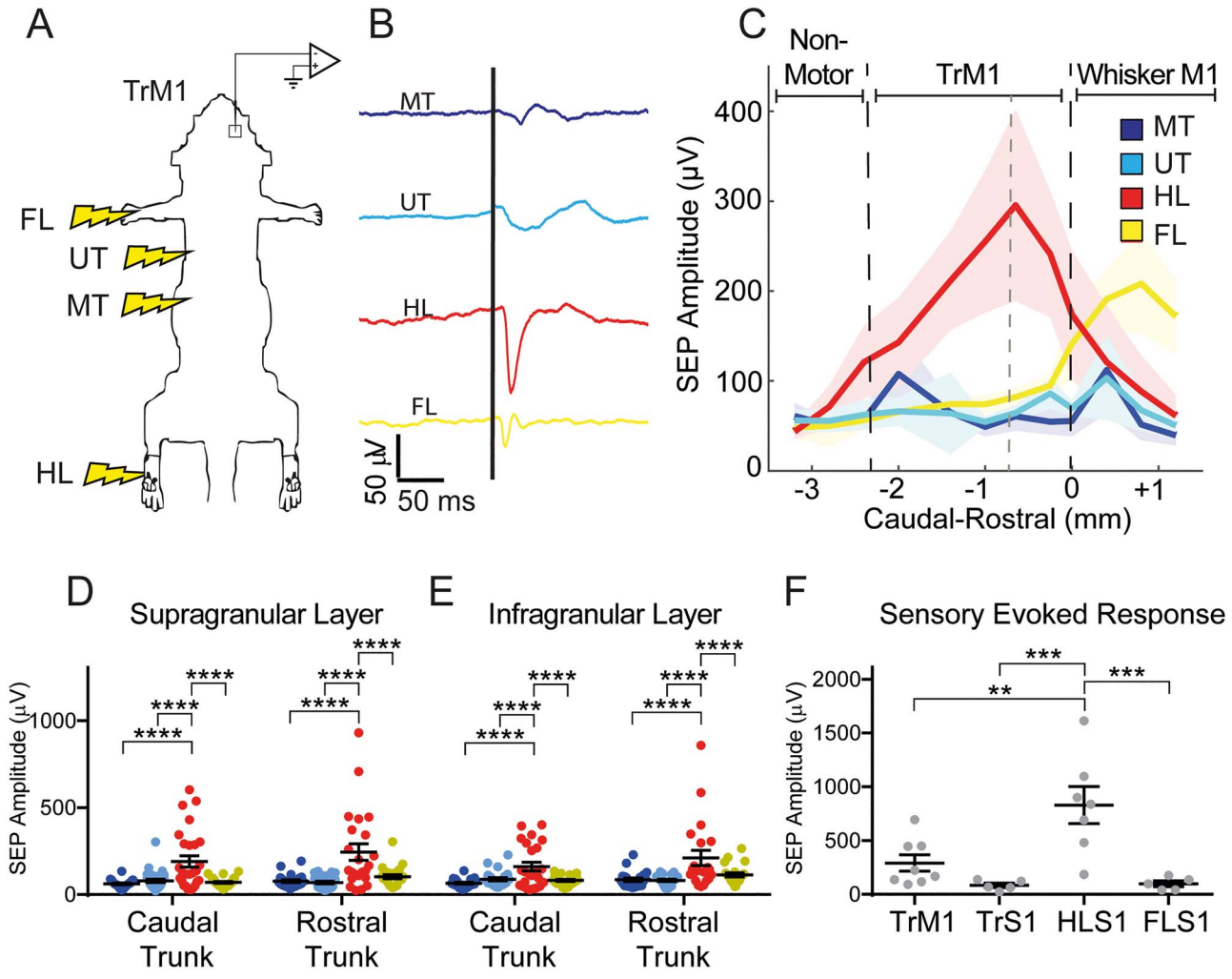

Figure 6. Response to high intensity hindlimb stimulation predominates in trunk M1. (A) Methodological diagram of the 5.0 mA electrical stimulation paradigm. Stimulations occurred in the dorsal hairy skin of forelimb (FL), hindlimb (HL), T4–T5 dermatome (UT), and T9–T10 dermatome (MT). (B) Example of somatosensory evoked responses in TrM1 from the different stimulation locations on the body. (C) SEP amplitude in the supragranular layer in response to stimulation across the rostrocaudal axis of TrM1 at 1.25 mm ML. Dotted line within TrM1 represents the distinction between caudal and rostral trunk. (D–E) SEP amplitude in the supragranular (Caudal $N = 103$; Rostral $N = 96$) (D) and infragranular (Caudal $N = 95$; Rostral $N = 85$) (E) layers in the caudal region (−1 mm to −2 mm RC, relative to bregma) and in the rostral region (−0.75 mm to 0 mm RC, relative to bregma) of the TrM1. Rostral regions activate upper thoracic musculature, whereas caudal regions activate lower thoracic trunk musculature. (F) Somatosensory evoked response in the supragranular layer of TrM1 ($N = 8$), TrS1 ($N = 5$), HLS1 ($N = 7$), and FLS1 ($N = 5$) from hindlimb stimulation.

role for hindlimb somatosensory integration within TrM1, but without any somatotopic organization. Surprisingly, there was no difference in the SEP amplitude in response to upper trunk stimulation compared to mid trunk stimulation (Tukey's post hoc test, $P = 0.99$), suggesting no somatotopy of trunk somatosensory input within TrM1.

In the infragranular layer (Caudal $N = 95$; Rostral $N = 85$), there was again an overall effect of stimulus location (Two-way ANOVA, F [3172] $= 14.48$, $P < 0.0001$; Fig. 6E), where the SEP amplitude to hindlimb stimulation was again greater in both the caudal and rostral region of TrM1 suggesting that hindlimb somatosensory input to TrM1 was evenly distributed, across supra- and infragranular layers, between LTM1 and UTM1 as suggested by Figure 6C. Moreover, like the supragranular layer, there were no differences between SEP amplitude in response to mid trunk stimulation compared to upper trunk stimulation (Tukey's post hoc test, $P = 0.95$), suggesting similar organization for both supra and infragranular layers. Finally, to assess the effectiveness of high intensity (5.0 mA) hindlimb stimulation to reach the sensory or motor cortices, the SEP amplitude was compared across TrM1 ($N = 8$), TrS1 ($N = 5$), HLS1 ($N = 7$), and FLS1 ($N = 5$). There was an overall effect of cortical location (One-way ANOVA, F [3, 21] $= 10.14$, $P < 0.001$; Fig. 6F), and as expected, the SEP response in HLS1 was greater than the response in any other region (Tukey's post hoc test, HLS1 vs. TrS1, $P < 0.001$; HLS1 vs. TrM1, $P < 0.01$; HLS1 vs. FLS1, $P < 0.001$). These results further support the extensive and preferential integration of hindlimb somatosensory input into TrM1.

Sensorimotor Integration Is Corticocortical for Trunk Stimuli, Thalamocortical for Hindlimb Stimuli

Since sensorimotor integration in the cortex can be mediated by projections from the S1 cortex and the thalamus

(Canedo 1997; Mao et al. 2011; Hooks 2016), retrograde tracing was used to better understand the relative contribution of corticocortical versus thalamocortical connections to TrM1 (Fig. 7A). Tracer injected into the location most likely to contain the exclusively trunk region revealed that TrM1 received corticocortical input from ipsilateral TrS1, HLS1, and FLS1. As expected, given the variability across animals in the location of exclusively trunk cortex, the relative contribution from these sensory cortices was variable across animals (Fig. 7B). Rats 1 and 2 had more cells projecting to TrM1 from HLS1 than from TrS1, whereas rat 3 showed projections exclusively from dorsal TrS1, and rats 4 and 5 showed projections predominately from dorsal TrS1. TrM1 also received input from secondary sensory cortex, dysgranular zone, whisker, and face S1 (data not shown), thereby making TrM1 a crossroad for somatosensory information.

In all animals, the projections from S1 to TrM1 were predominantly mediated by S1 cells in the supragranular and infragranular layers (Fig. 7C). This laminar specificity is consistent with studies in the whisker sensorimotor system (Mao et al. 2011; Hooks et al. 2013). Tracing also revealed strong thalamocortical projections from the ventral posterolateral nucleus (VPL) of the thalamus to TrM1 in all animals (Fig. 7D and E) that likely carries proprioceptive information (Francis et al. 2008), however, tactile information from the thalamus cannot be ruled out.

To determine if the source of projections to TrM1 differed between body parts that were stimulated, SEP latency was analyzed. The mean latency of the SEP recorded from TrM1 (26.84 ± 2.65 ms) was significantly longer than that from TrS1 (20.30 ± 0.83 ms) when mid trunk was stimulated (Independent Samples t-test, t [12] $= 2.66$, $P < 0.05$; Fig. 7F). This led us to conclude that the sensorimotor integration of trunk somatosensory information in TrM1 is primarily mediated by corticocortical projections. In contrast, the mean latency of the SEP recorded from TrM1 (23.44 ± 1.81 ms) was similar to the that from HLS1 (21.15 ± 1.66 ms) when hindlimb was stimulated (Independent Samples t-test, t [12] $= 0.90$, $P = 0.39$; Fig. 7F and see Supplementary Fig. 3). This led us to conclude that the integration of hindlimb somatosensory input in TrM1 is primarily mediated by thalamocortical projections, carrying somatosensory information, including proprioceptive. To identify how this somatosensory information might be used, next we recorded single neurons from TrS1 and TrM1 while animals were subjected to tilts in the lateral plane.

Postural Control Is Predominately Supported by Hindlimb Somatosensory and Lower Trunk Motor Cortices

To investigate the importance of sensorimotor integration between trunk and hindlimb in postural control, animals were subjected to unexpected tilts in the lateral plane during a tilt task (Bridges et al. 2018), while single units were recorded from the following S1 and M1 cortices: FLS1 ($n = 68$), HLS1 ($n = 39$), TrS1 ($n = 237$), HLM1 ($n = 124$), and TrM1 ($n = 325$; Fig. 8A and B). Three measures from the neuronal data were compared: responsiveness (i.e., proportion of neurons responding), magnitude of the single neuron response, and mutual information carried by the response regarding the severity of the tilt (Fig. 8C–H). First, the proportion of responsive cells was compared between S1 regions (FLS1: 57%, TrS1: 32%, HLS1: 82%). TrS1 was less responsive than HLS1 (χ^2 [1, $N = 276$] $= 35.84$, $P < 0.0001$) or FLS1 (χ^2 [1, $N = 305$] $= 14.92$, $P < 0.001$), and HLS1 cells were more likely to respond than FLS1 (χ^2 [1, $N = 107$] $= 6.77$, $P < 0.01$; Fig. 8C). Moreover, the magnitude of the TrS1 response (1.87 ± 0.19 spikes per second) was smaller than that of HLS1 (3.32 ± 0.36 spikes per second) or FLS1 cells (2.94 ± 0.32 spikes per second) during the tilt task (One-way ANOVA, F [2, 145] $= 8.63$, $P < 0.001$, Tukey's post hoc test: HLS1 vs. TrS1 [$P < 0.001$], FLS1 vs. TrS1 [$P < 0.05$]; Fig. 8D). Lastly, mutual information was compared between S1 regions. The median mutual information carried by TrS1 (0.04, [0.03] bits) was significantly less than the median mutual information carried by FLS1 (0.05 [0.06] bits) or HLS1 (0.06 [0.07] bits) during the tilt task (Kruskal–Wallis test, H [2] $= 21.73$, $P < 0.0001$, Dunn's post hoc test: HLS1 vs. TrS1 [$P < 0.001$], FLS1 vs. TrS1 [$P < 0.01$]; Fig. 8E). Thus, TrS1 conveyed less mutual information and was less discriminative of the type of tilt than FLS1 or HLS1. Importantly, after dividing TrS1 into LT, MT, and UT (see Materials and Methods), there were no differences between these trunk subregions in responsiveness (LTS1: 50%, MTS1: 38%, UTS1: 28%; χ^2 [2, $N = 237$] $= 5.64$, $P = 0.06$). The magnitude of response significantly differed between these TrS1 subregions (LTS1: 2.25 [1.93], MTS1: 0.88 [1.23], UTS1: 1.59 [1.59]; Kruskal–Wallis test, H [3] $= 6.67$, $P < 0.05$); however, Dunn's post hoc test did not reveal any significant pairwise comparisons. Additionally, there were no differences in mutual information between subregions (LTS1: 0.04 ± 0.004, MTS1: 0.06 ± 0.01, UTS1: 0.06 ± 0.01; One-way ANOVA, F [2, 234] $= 0.43$, $P = 0.65$; Fig. 8C–E), suggesting that the entire TrS1 is equally engaged in this task.

On the other hand, TrM1 neurons were equally likely to respond to the task compared to HLM1 neurons (HLM1: 63%, TrM1: 72%; Fisher's exact test, $N = 449$, $P = 0.07$; Fig. 8F), though neither the magnitude of the response (HLM1: 3.42 ± 0.30 spikes per second, TrM1: 4.05 ± 0.23 spikes per second; Independent Samples t-test, t [311] $= 1.46$, $P = 0.14$; Fig. 8G), nor their mutual information (HLM1: 0.07 [0.08] bits, TrM1: 0.06 [0.08]; Mann–Whitney test, $U = 19\,112$, $P = 0.40$; Fig. 8H) differed from HLM1. Interestingly, when examining the responses from different subregions within TrM1, LTM1 was more involved than UTM1. In fact, even though neurons in LTM1 had a similar proportion of cells responding to the tilts compared to UTM1 (LTM1: 76%, UTM1: 69%; χ^2 [1, $N = 325$] $= 2.32$, $P = 0.12$; Fig. 8F), the magnitude of the response of LTM1 neurons was greater than that of UTM1 neurons (LTM1: 4.57 ± 0.35, UTM1: 3.46 ± 0.27; Independent Samples t-test, t [233] $= 2.49$, $P < 0.05$; Fig. 8G). This resulted in more information about the severity of the tilt being encoded by LTM1 compared to UTM1 (LTM1:0.07 [0.09] bits, UTM1: 0.06 [0.06] bits; Mann–Whitney test, $U = 11\,063$, $P < 0.05$; Fig. 8H). These data suggest that LTM1 may be specialized for postural control.

Discussion

Together, these data present an extensive view describing how cortical organization is relevant to function by demonstrating the preferential interplay between trunk and hindlimb (Fig. 9). Summarizing, TrS1 and TrM1 are larger than previously reported and there is relevant somatotopy within both. In addition, TrS1 receives input from other body regions, especially the hindlimbs, and TrM1 largely coactivates trunk muscles with muscles from other body regions, especially the hindlimbs. Regarding sensorimotor integration, somatosensory information from the hindlimbs is more likely to be integrated within TrM1 than that from forelimbs or even trunk. The functional role of this integration of hindlimb somatosensory information within

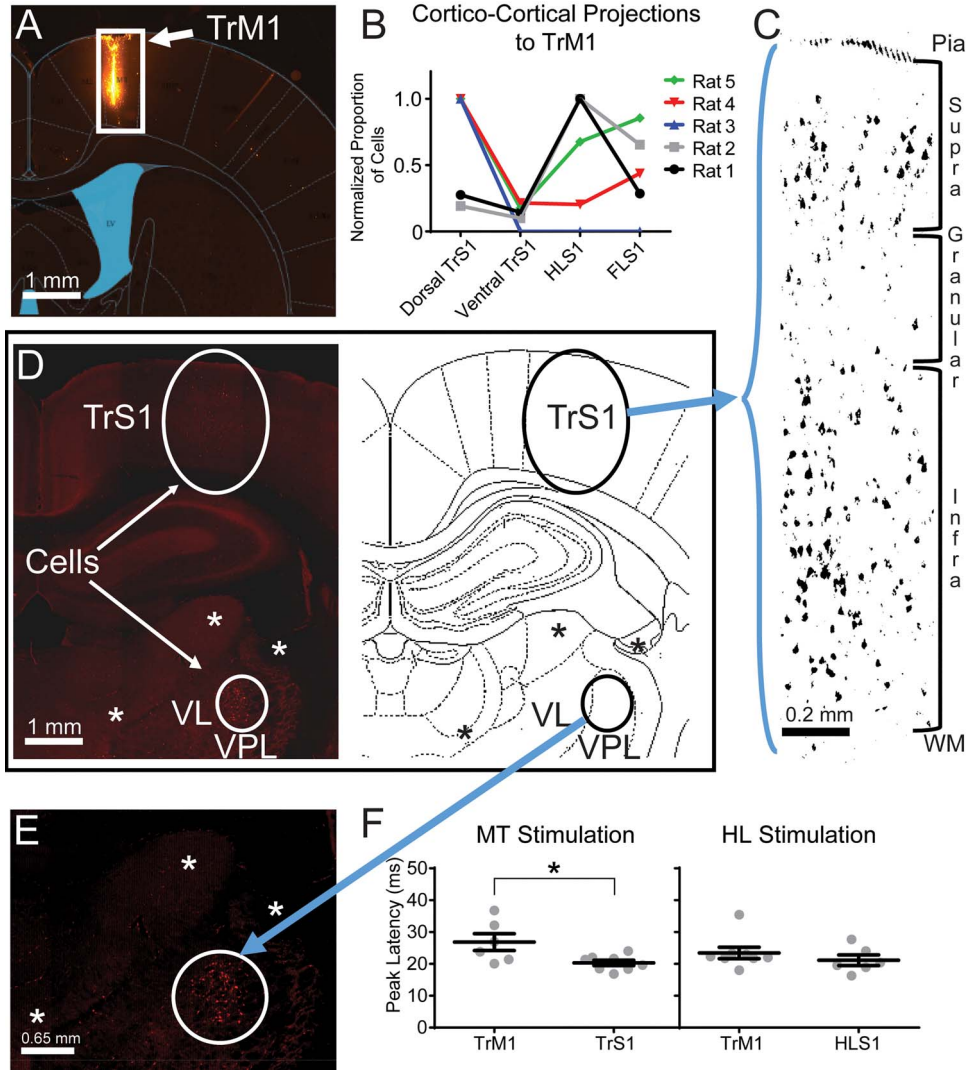

Figure 7. Corticocortical and thalamocortical projections to trunk M1. (A) Coronal brain slice with a superimposed rat brain atlas image (Paxinos and Watson 2007). The injection site (−0.5 mm RC, 1.25 mm ML, 1.65 mm DV, relative to bregma) was limited to TrM1. Scale bar: 1 mm. (B) Proportion of cells, normalized to the maximum number of cells across all cortical regions sampled within an animal, in the different primary sensory cortices (dorsal trunk S1, ventral trunk S1, hindlimb S1, and forelimb S1; for coordinates see Materials and Methods). Most TrM1 projecting cells are located in TrS1 and HLS1. (Rat number: raw number of cells in dorsal TrS1, ventral TrS1, HLS1, and FLS1; Rat 1: 229, 120, 830, 237; Rat 2: 62, 32, 323, 211; Rat 3: 257, 0, 0, 0; Rat 4: 1886, 404, 384, 826; Rat 5: 1344, 236, 908, 1149.) (C) Black and white image of the labeled cortical cells in a coronal view of TrS1. Most of the neurons are located in the supra- and infragranular layers. Scale bar: 0.2 mm. (D) Image of the labeled cortical and thalamic cells in a coronal view with the corresponding modified rat brain atlas. Thalamic neurons are located in the VPL of the thalamus as the thalamic nuclei borders can be seen in both the left image and in the right atlas. The "*" indicates corresponding structures to help the viewer localizing the different thalamic nuclei. Scale bar: 1 mm. (E) Zoomed in image of D to visualize the labeled cells in the VPL of the thalamus. The contrast has been increased in order to specifically focus on the presence of the labeled cells. The "*" indicates the same locations as in D to aid the viewer in locating the cells. Scale bar: 0.65 mm. (F) Left: peak latency of the high intensity mid trunk stimulation in TrM1 ($N = 6$) and TrS1 ($N = 8$). Right: peak latency of the high intensity hindlimb stimulation in TrM1 ($N = 8$) and HLS1 ($N = 6$).

TrM1 for postural control was demonstrated by the relative difference in the mutual information carried by hindlimb and trunk sensory and motor cortices to tilts in the lateral plane recorded from awake animals. On the sensory side, HLS1 and FLS1 are more involved than TrS1 during postural perturbations. Although on the motor side, HLM1 and TrM1 are equally involved, with LTM1 more involved than UTM1. This has important implications for recovery of function after neurological injury or disease (Knudsen and Moxon 2017; Manohar et al. 2017; Bridges et al. 2018) and is discussed below.

Methodological Considerations

Choices made in our experimental design impacted data analysis. First, for sensory maps, we chose to record from as many single units as possible, identifying the extent of each cell's RF as our recording electrode was passed through the entire depth of S1. Therefore, it was not possible to sample the entire TrS1 within a single animal due to time constraints. Similarly, for TrM1, we chose to sample from as many muscles as possible, adding to the length of the surgery and limiting our ability to sample the entire TrM1 within every animal. Moreover, here we show that, unlike the

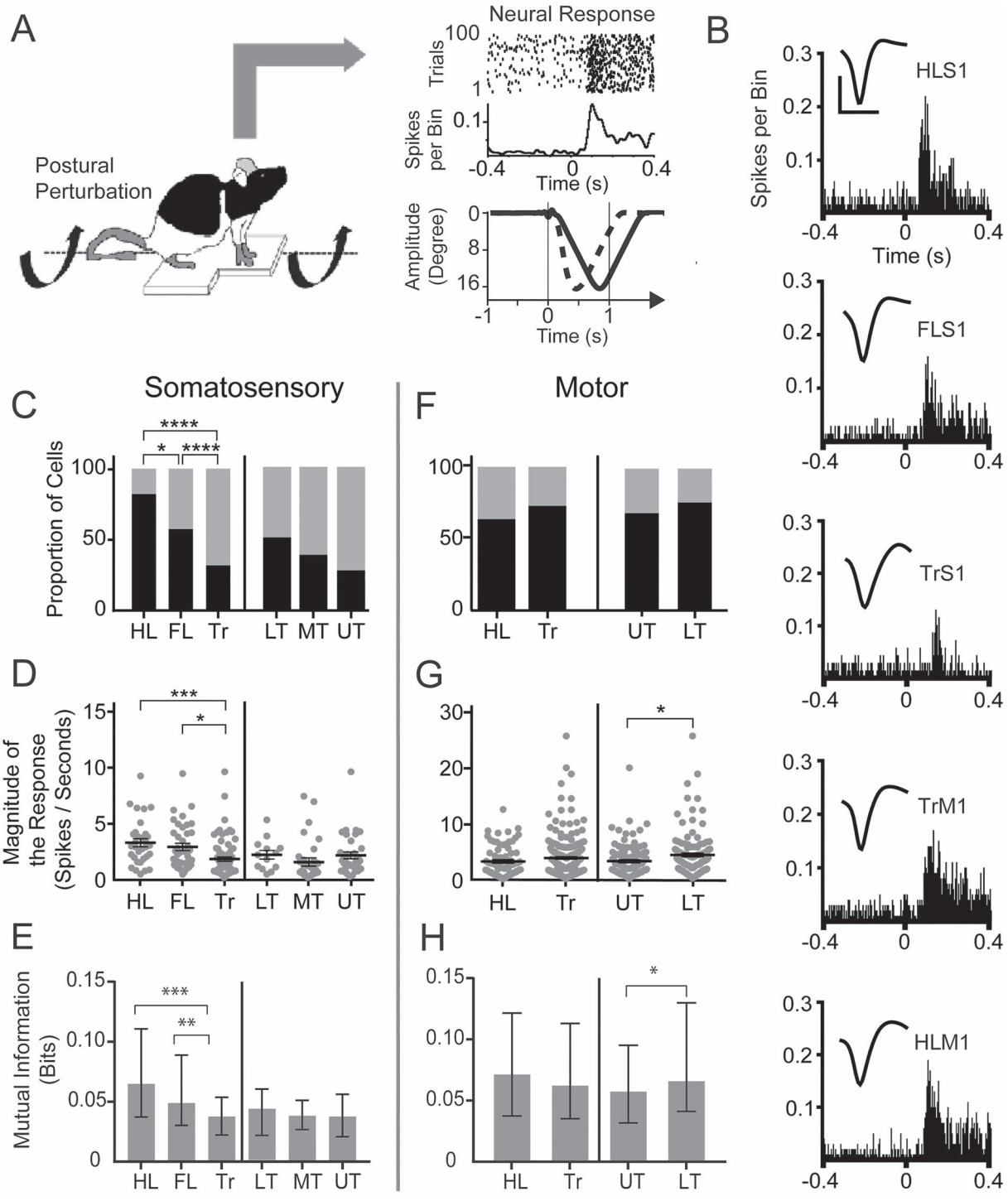

Figure 8. Hindlimb S1 and lower trunk M1 combine to carry the most information about postural control. (A) Methodological diagram of the postural control task. The animal experienced unexpected tilts in the lateral plane while single neurons in different sensory and motor cortices were recorded (upper right panel). The bottom right panel shows the tilt profile for the fast (dotted line) and the slow (unbroken line) tilt events, applicable for both directions (left and right). (B) Example PSTHs showing a neuron response to the unexpected tilt for each recorded cortical area in the sensory and motor cortices. The waveform scale on top: *y*-axis: 0.05 mV, *x*-axis: 0.6 ms. (C) Responsiveness of different sensory cortices. Data presented as cortical area: (number of responsive cells, number of nonresponsive cells, % of responsive cells). HLS1: (32, 7, 82%), FLS1: (39, 29, 57%), TrS1: (80, 157, 34%), LT: (13, 13, 50%), MT: (31, 51, 38%), UT: (36, 93, 28%). (D) Magnitude of the response (for responsive cells only) in different sensory cortices. (E) Mutual information in different sensory cortices (represented as median ± interquartile range for all cells [responsive and nonresponsive]). (F) Responsiveness of different motor cortices. Data presented as: cortical area (number of responsive cells, number of nonresponsive cells, % of responsive cells). HLM1 (78, 46, 63%), TrM1 (235, 90, 72%), LTM1 (111, 51, 76%), UTM1 (124, 39, 69%). (G) Magnitude of the response (for responsive cells only) in different motor cortices. (H) Mutual information in different motor cortices (represented as median ± inter quartile range for all cells [responsive and nonresponsive]).

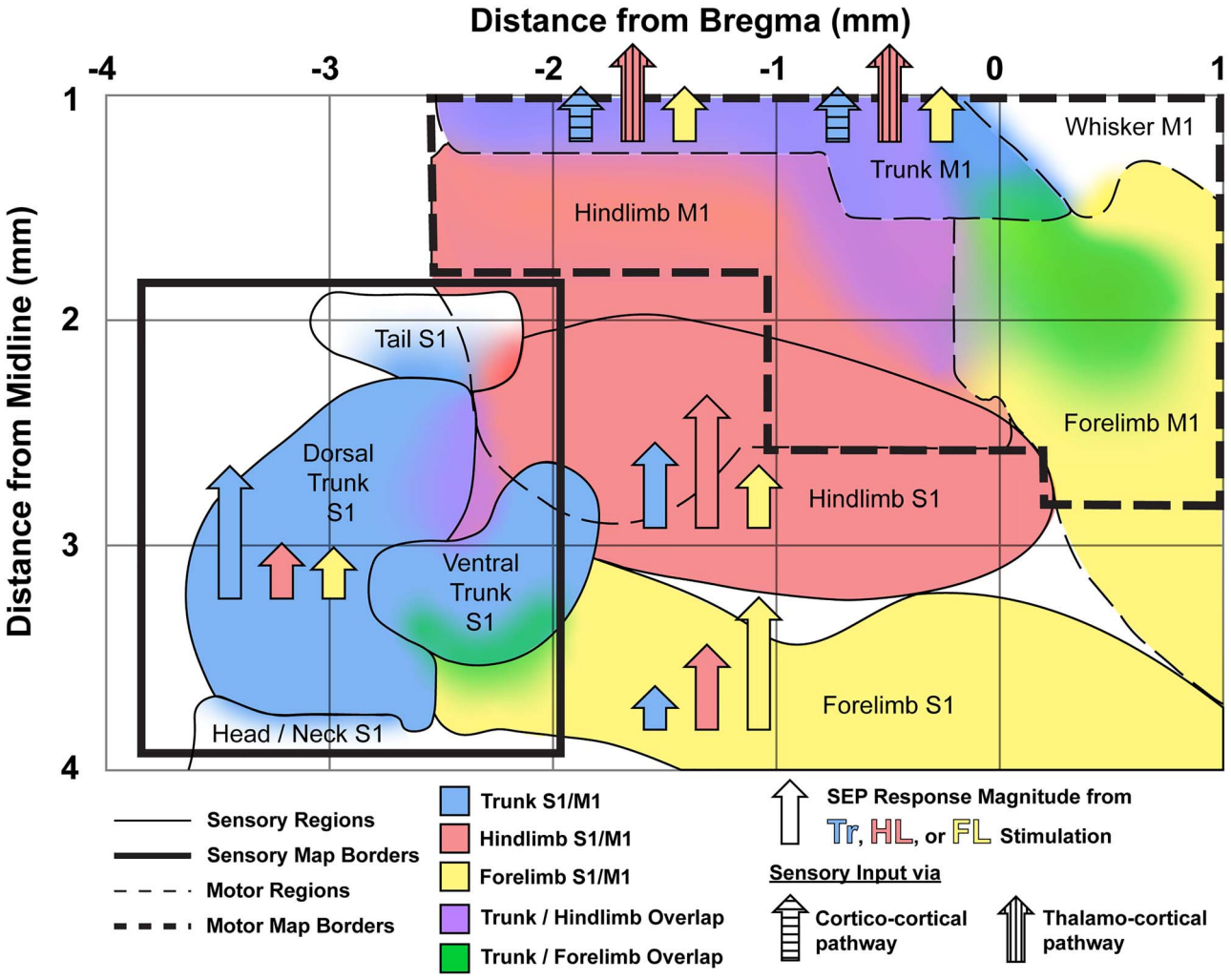

Figure 9. Summary of somatosensory overlap, motor coactivations, and sensorimotor integration. Solid border lines indicate sensory regions whereas dashed border lines indicate motor regions. Bolded lines indicate the areas of S1 and M1 that were mapped in the current study. All other regions outside of these areas were adapted from (Xerri et al. 1994) and (Leergaard et al. 2004). Corresponding S1/M1 regions (e.g., trunk S1/trunk M1) are represented with the same colors, whereas overlapping S1 regions or coactivating M1 regions are represented by the combined colors of the neighboring regions. Arrow height represents the relative magnitude of SEP responses within each cortical region from 5.0 mA stimulation of the trunk (blue), hindlimb (red), and forelimb (yellow). Horizontal (corticocortical) and vertical (thalamocortical) stripe patterns within each stimulation type's arrow indicates the predominate pathway for that type of sensory information to reach TrM1.

whisker, forelimb, and hindlimb sensory systems that tend to have differences in RF size across layers (Chapin 1986), the RF size of neurons in TrS1 was similar across layers, within the same RF center. However, the role of urethane anesthesia in this assessment cannot be ruled out (Friedberg et al. 1999). Furthermore, within S1, the responses to both low- and high-intensity stimuli are likely to be a combination of tactile and proprioceptive information, with the low-intensity stimulation predominately eliciting tactile information and the high-intensity stimulation adding additional proprioceptive information. In comparison to S1, low-intensity stimuli did not elicit responses within M1; however, high-intensity stimuli induced muscle twitches. Thus, in M1, a greater proportion of responses to high-intensity stimuli were likely proprioceptive than tactile. The tracing study suggests that somatosensory information, a mix of tactile and proprioceptive information, reaches TrM1 from S1 and thalamus. The latency studies suggest that the predominate response in TrM1 to mid trunk stimulation arrives from the somatosensory cortex. Alternatively, the predominate response in TrM1 that is elicited by hindlimb stimulation likely arrives from the VPL of the thalamus. The VPL origin of this response, which predominately carries proprioceptive information, further supports that the response in TrM1 to high-intensity stimulation of the hindlimbs carries more proprioceptive information than the low-intensity stimulation, although more work would need to be done to confirm this.

Oppositional Gradient in Overlap across Thoracic Dermatomes from DRG to Trunk S1

Overlap of somatosensory information from the trunk varies along the entire neural axis. At the spinal level, overlap between thoracic dermatomes is graded such that caudal DRGs (T10–T13) have less overlap than rostral DRGs (T1–T5). At the same time, representation of these dermatomes in S1 has the opposite gradient regarding overlap. The RF size of TrS1 neurons increased along the ML axis of cortex, such that the lower thoracic TrS1 neurons had a greater RF size compared to the upper thoracic TrS1 neurons. This change in RF size across TrS1

has also been shown in the ventral trunk representation (Xerri et al. 1994). Taken together, for a given stimulation to lower trunk dermatomes, the limited overlap results in fewer DRGs conveying somatosensory information to the cortex where S1 neurons with larger RFs amplify the signal. In contrast, for upper trunk dermatomes, the greater overlap across DRGs amplifies information to the cortex where neurons have smaller RFs. Therefore, the lack of overlap at the spinal level is compensated for by the greater overlap at the cortical layer and vice versa. The functional implication of this is that dorsal rhizotomy of a caudal DRG would result in a more complete deafferentation than a dorsal rhizotomy of a rostral DRG. It may be that due to the dexterous use of the forelimbs, it is considered more important to preserve upper trunk than lower trunk somatosensory information.

Trunk Sensorimotor Integration Supports a Range of Functions

The present data suggest that trunk muscles serve as a biomechanical link between the forelimbs and hindlimbs even in the absences of a neonatal spinal cord transection (Giszter et al. 2010). Moreover, this linkage combines somatosensory information across the limbs and trunk, especially the hindlimbs. In the intact adult, our data show extensive overlap of trunk somatosensory signals within FLS1 and HLS1, especially in response to high-intensity stimuli, thereby suggesting that HLS1 is modulated by the location and movement of trunk in space, which could be used to guide the lower limbs during locomotion (Rossignol et al. 2006). At the same time, somatosensory information from hindlimb and forelimb overlap within TrS1, which confirms the importance of integrating information from the limbs with trunk somatosensory processing. Within M1, trunk muscles are more likely to coactivate with hindlimb than trunk muscles or forelimb muscles alone. Furthermore, approximately half of the animals had coactivation of forelimb and hindlimb muscles without concomitant activation of trunk muscles (data not shown). The area was located within the synergistic trunk region. This coactivation of forelimb and hindlimb was also found in other species across phylogenic scales, such as the mouse (Li and Waters 1991), tree squirrel (Cooke et al. 2012), tree shrew (Baldwin et al. 2017), prosimian Galagos (Stepniewska et al. 2005), and macaque monkey (Baldwin et al. 2018). These synchronous forelimb–hindlimb coactivations (Halley et al. 2020) are thought to be involved in a range of movement types associated with locomotion (e.g., galloping; Lemieux et al. 2016). The work presented here extends this understanding by highlighting the greater integration between trunk and hindlimb than trunk and forelimb.

Classical studies showed that sensory information in M1 was mainly homotopic. For example, neurons in whisker M1, FLM1, and HLM1 received somatosensory input from the same body part that induced movement when activated with ICMS (Asanuma et al. 1968; Rosén and Asanuma 1972). However, our data suggest that the TrM1 is unique in that it receives somatosensory information from trunk, hindlimbs, and forelimbs, and therefore the integration of sensorimotor information within TrM1 is not strictly homotopic. Indeed, whereas low amplitude somatosensory stimulation of trunk, hindlimb, or forelimb did not impact TrM1, high-amplitude stimulation of HL produced a greater response in TrM1 than somatosensory stimulation of either trunk or forelimb. As many studies have demonstrated that somatosensory feedback to the motor cortex is critical during locomotion and recovery of function after spinal cord injury (Hicks and D'Amato 1975; Rossignol et al. 2006; Beaumont et al. 2014; Moreno-López et al. 2016; Knudsen and Moxon 2017; Manohar et al. 2017), understanding how the postinjury sensorimotor integration differs from the integration shown here will be important for interpreting these injury studies.

Combined, this extensive sensory overlap, muscle coactivations, and heterotopic sensory integration between the trunk and the limbs supports communication between trunk sensory and motor cortices within the broader sensorimotor cortex to achieve optimal behavior. For example, it has been previously shown that the lower thoracic trunk muscles play an important role in sexual posturing and lordosis as observed in the female rat (Brink and Pfaff 1980). Our results show that the caudal portion of TrM1 that controls these lower thoracic muscles overlaps with the genital motor cortex (Lenschow and Brecht 2018). The extensive integration of hindlimb somatosensory information within TrM1 could be useful for sexual posturing.

Role of Trunk Sensorimotor Cortex in Postural Control

The integration of HL somatosensory input across the extent of TrM1combined with the broad hindlimb–trunk coactivation zones in M1 support the role of thoracic trunk muscles synergistically acting with the hindlimbs to aid in postural control during locomotion (Anders et al. 2007; Song et al. 2015; Bridges et al. 2018). This coactivation likely happens through the cortico–reticulo–spinal pathway, not directly via the corticospinal pathway. In the awake animal, the vestibular system, which was not studied here, produces a fast reaction to control posture and recover balance (Murray et al. 2018). Notably, it sends direct motor inputs to the spinal cord to correct the balance. This vestibular information also ascends through the thalamus to the motor cortex to produce a coordinated neuronal response across the body musculature during the tilt (Horak and Jacobs 2007; Whelan 2009). Interestingly, the motor cortex participates in some, but not all, aspects of postural control (Deliagina et al. 2007; Horak and Jacobs 2007), producing different responses depending on the task despite similar muscle output (Karayannidou et al. 2009). Given the critical role of M1 for functional improvement after SCI (Manohar et al. 2017), improving our understanding of how information about postural adjustments is integrated in M1 will aid in understanding how M1 contributes to recovery of function (see next section).

For example, in S1, previous studies showed that tactile and proprioceptive somatosensory feedback from the limbs are involved in postural control (Deliagina and Beloozerova 2000; Beloozerova et al. 2003). This is consistent with our data here showing that for both HLS1 and FLS1, more cells respond, and the magnitude of their response was greater compared to that of TrS1, such that FLS1 and HLS1 convey more information about the tilt than TrS1. But, within TrS1, the different areas of trunk (LT, MT, and UT) are equally responsive, conveying similar amounts of information about tilt. We can deduce that the response in TrS1 is predominately mediated by trunk proprioceptive information because the trunk is not in contact with the platform. Furthermore, because this study showed that a significant proportion of neurons in TrS1 responded to HL somatosensory information during the tilt task, the somatosensory information reaching TrS1 comes from the position of both

the trunk and hindlimb in space, allowing significant integration of this proprioceptive information, along with tactile and vestibular, to allow the animal to maintain its balance.

In the motor cortex, a similar proportion of HLM1 and TrM1 cells were likely to respond with a similar magnitude of response, conveying a similar amount of information about the tilt, suggesting that these two regions are equally active in controlling muscles when the animal is maintaining its balance in response to the tilt. Interestingly, within TrM1, the region that controls lower thoracic muscles (LTM1) was more engaged in the task compared to the regions that control upper thoracic musculature (UTM1). Given that more of the weight of the animal is over the hindlimbs, these data suggest that extensive coactivation across hindlimb and lower thoracic muscles is used for postural control.

Hindlimb Somatosensory Feedback to the Trunk Motor Cortex: Pathophysiological Implications

Pathologies resulting in postural deficits in humans are associated with changes in cortical organization (Tsao et al. 2008), motor planning (Hodges 2001), and recruitment of trunk musculature (Tsao et al. 2011). The integration of hindlimb proprioceptive information in TrM1 cortex identified here provides an opportunity for a new understanding of how therapy after mid thoracic spinal cord injury improves function. For a complete spinal transection, we previously showed that therapy produced sprouting of descending corticospinal axons from HLM1 cortex into thoracic spinal cord that could be used to control trunk musculature. This produced a larger representation of the TrM1 cortex whose extent was correlated to recovery of function and overlapped with expansion of the FLS1, creating a new circuit of forelimb somatosensory and trunk motor integration (Ganzer et al. 2016). If this reorganized cortex was lesioned, functional gains were lost (Manohar et al. 2017). Our new understanding of the extensive sensorimotor integration in intact animals presented here makes it more clear that the sensorimotor integration in animals that receive therapy after SCI is not a novel sensorimotor integration, but a necessary restoration of a system that operates on strong sensorimotor organization.

Although the role of limb proprioception after more severe injuries is less understood, our group previously showed that after complete spinal transection, when somatosensory input from the hindlimb is not possible, epidural stimulation induces somatosensory feedback from the trunk into the deafferented hindlimb sensorimotor cortex that carries information about the animal's behavior (Knudsen and Moxon 2017). This study now makes clear that this somatosensory feedback is likely to be trunk proprioceptive information that provides input to hindlimb S1 and M1 cortices in intact animals. Therefore, therapy to improve function could take advantage of this pre-existing sensorimotor integration to restore function.

This role of sensorimotor integration extends to models of partial spinal lesion. Proprioceptive information has been suggested to be critical for recovery of function after mid thoracic spinal cord injury (Edgerton et al. 2008). For example, epidural stimulation of spinal circuitry below the level of the lesion restored volitional locomotion in rats (Van Den Brand et al. 2012; Knudsen and Moxon 2017; Asboth et al. 2018), nonhuman primates (Capogrosso et al. 2016), and humans (Harkema et al. 2011; Rejc et al. 2017; Formento et al. 2018). Stimulation is conducted at lateral sites, over or near the DRGs and it has been suggested that this epidural stimulation activates proprioceptive afferents (Takeoka et al. 2014; Formento et al. 2018).

Therefore, the work outlined in this paper supports the idea that facilitation of sensorimotor integration across broad regions of the cortex is key to improving treatment outcomes after neurological damage or disease (Ingemanson et al. 2019) and we now understand that this sensorimotor integration is the operational model of the trunk cortex in intact animals. Moving forward, our understanding of the sensorimotor integration in the intact system could be used to tailor rehabilitative strategies to optimize sensorimotor integration or recovery of function.

Supplementary Material

Supplementary material can be found at *Cerebral Cortex* online.

Notes

Conflict of Interest: None declared.

Funding

This work was supported by grant R01NS096971 from the National Institutes of Health and grant 1933751 from the National Science Foundation.

References

Anders C, Wagner H, Puta C, Grassme R, Petrovitch A, Scholle HC. 2007. Trunk muscle activation patterns during walking at different speeds. *J Electromyogr Kinesiol*. 17:245–252.

Asanuma H, Stoney SD Jr, Abzug C. 1968. Relationship between afferent input and motor outflow in cat motorsensory cortex. *J Neurophys*. 31:670–681.

Asboth L, Friedli L, Beauparlant J, Martinez-Gonzalez C, Anil S, Rey E, Baud L, Pidpruzhnykova G, Anderson MA, Shkorbatova P *et al*. 2018. Cortico–reticulo–spinal circuit reorganization enables functional recovery after severe spinal cord contusion. *Nat Neurosci*. 21:576–588.

Baldwin MKL, Cooke DF, Goldring AB, Krubitzer L. 2018. Representations of fine digit movements in posterior and anterior parietal cortex revealed using long-train intracortical microstimulation in macaque monkeys. *Cereb Cortex*. 28:4244–4263.

Baldwin MKL, Cooke DF, Krubitzer L. 2017. Intracortical microstimulation maps of motor, somatosensory, and posterior parietal cortex in tree shrews (tupaia belangeri) reveal complex movement representations. *Cereb Cortex*. 27:1439–1456.

Beaumont E, Guevara E, Dubeau S, Lesage F, Nagai M, Popovic M. 2014. Functional electrical stimulation post-spinal cord injury improves locomotion and increases afferent input into the central nervous system in rats. *J Spinal Cord Med*. 37:93–100.

Beloozerova IN, Sirota MG, Swadlow HA, Orlovsky GN, Popova LB, Deliagina TG. 2003. Activity of different classes of neurons of the motor cortex during postural corrections. *J Neurosci*. 23:7844–7853.

Blumenthal GH, Nandakumar B, Schnider AK, Detloff MR, Ricard J, Bethea JR, Moxon KA. 2021. Modelling at-level allodynia after mid-thoracic contusion in the rat. *Eur J Pain*. 25:801–816.

Boyeson MG, Feeney DM, Dail WG. 1991. Cortical microstimulation thresholds adjacent to sensorimotor cortex injury. *J Neurotrauma*. 8:205–217.

Bridges NR, Meyers M, Garcia J, Shewokis PA, Moxon KA. 2018. A rodent brain-machine interface paradigm to study the impact of paraplegia on BMI performance. *J Neurosci Methods*. 306:103–114.

Brink EE, Pfaff DW. 1980. Vertebral muscles of the back and tail of the albino rat (Rattus norvegicus albinus). *Brain Behav Evol*. 17:1–47.

Brown AR, Teskey GC. 2014. Motor cortex is functionally organized as a set of spatially distinct representations for complex movements. *J Neurosci*. 34:13574–13585.

Canedo A. 1997. Primary motor cortex influences on the descending and ascending systems. *Prog Neurobiol*. 51:287–335.

Capogrosso M, Milekovic T, Borton D, Wagner F, Moraud EM, Mignardot JB, Buse N, Gandar J, Barraud Q, Xing D *et al*. 2016. A brain-spine interface alleviating gait deficits after spinal cord injury in primates. *Nature*. 539:284–288.

Chakrabarti S, Zhang M, Alloway KD. 2008. MI neuronal responses to peripheral whisker stimulation: relationship to neuronal activity in SI barrels and septa. *J Neurophysiol*. 100:50–63.

Chapin JK. 1986. Laminar differences in sizes, shapes, and response profiles of cutaneous receptive fields in the rat SI cortex. *Exp Brain Res*. 62:549–559.

Chapin JK, Lin CS. 1984. Mapping the body representation in the SI cortex of anesthetized and awake rats. *J Comp Neurol*. 229:199–213.

Clement EA, Richard A, Thwaites M, Ailon J, Peters S, Dickson CT. 2008. Cyclic and sleep-like spontaneous alternations of brain state under urethane anaesthesia. *PLoS One*. 3:e2004.

Cooke DF, Padberg J, Zahner T, Krubitzer L. 2012. The functional organization and cortical connections of motor cortex in squirrels. *Cereb Cortex*. 22:1959–1978.

Deliagina TG, Beloozerova IN. 2000. Role of different sensory inputs for maintenance of body posture in sitting rat and rabbit. *Motor Control*. 4:439–452.

Deliagina TG, Zelenin PV, Beloozerova IN, Orlovsky GN. 2007. Nervous mechanisms controlling body posture. *Physiol Behav*. 92:148–154.

Donoghue JP, Kerman KL, Ebner FF. 1979. Evidence for two organizational plans within the somatic sensory-motor cortex of the rat. *J Comp Neurol*. 183:647–663.

Donoghue JP, Wise SP. 1982. The motor cortex of the rat: cytoarchitecture and microstimulation mapping. *J Comp Neurol*. 212:76–88.

Edgerton VR, Courtine G, Gerasimenko Y, Lavrov I, Ichiyama R, Fong AJ, Cai LL, Otoshi CK, Tillakaratne NJK, Burdick JW *et al*. 2008. Training locomotor networks. *Brain Res Rev*. 57: 241–254.

Farkas T, Kis Z, Toldi J, Wolff JR. 1999. Activation of the primary motor cortex by somatosensory stimulation in adult rats is mediated mainly by associational connections from the somatosensory cortex. *Neuroscience*. 90:353–361.

Ferezou I, Haiss F, Gentet LJ, Aronoff R, Weber B, Petersen CCH. 2007. Spatiotemporal dynamics of cortical sensorimotor integration in behaving mice. *Neuron*. 56:907–923.

Foffani G, Chapin JK, Moxon KA. 2008. Computational role of large receptive fields in the primary somatosensory cortex. *J Neurophysiol*. 100:268–280.

Foffani G, Moxon KA. 2004. PSTH-based classification of sensory stimuli using ensembles of single neurons. *J Neurosci Methods*. 135:107–120.

Formento E, Minassian K, Wagner F, Mignardot JB, Le Goff-Mignardot CG, Rowald A, Bloch J, Micera S, Capogrosso M, Courtine G. 2018. Electrical spinal cord stimulation must preserve proprioception to enable locomotion in humans with spinal cord injury. *Nat Neurosci*. 21:1728–1741.

Francis JT, Xu S, Chapin JK. 2008. Proprioceptive and cutaneous representations in the rat ventral posterolateral thalamus. *J Neurophysiol*. 99:2291–2304.

Friedberg MH, Lee SM, Ebner FF. 1999. Modulation of receptive field properties of thalamic somatosensory neurons by the depth of anesthesia. *J Neurophysiol*. 81:2243–2252.

Frost SB, Dunham CL, Barbay S, Krizsan-Agbas D, Winter MK, Guggenmos DJ, Nudo RJ. 2015. Output properties of the cortical hindlimb motor area in spinal cord-injured rats. *J Neurotrauma*. 32:1666–1673.

Ganzer PD, Manohar A, Shumsky JS, Moxon KA. 2016. Therapy induces widespread reorganization of motor cortex after complete spinal transection that supports motor recovery. *Exp Neurol*. 279:1–12.

Ghosh A, Sydekum E, Haiss F, Peduzzi S, Zörner B, Schneider R, Baltes C, Rudin M, Weber B, Schwab ME. 2009. Functional and anatomical reorganization of the sensory-motor cortex after incomplete spinal cord injury in adult rats. *J Neurosci*. 29:12210–12219.

Gioanni Y, Lamarche M. 1985. A reappraisal of rat motor cortex organization by intracortical microstimulation. *Brain Res*. 344:49–61.

Girgis J, Merrett D, Kirkland S, Metz GAS, Verge V, Fouad K. 2007. Reaching training in rats with spinal cord injury promotes plasticity and task specific recovery. *Brain*. 130: 2993–3003.

Giszter S, Davies MR, Ramakrishnan A, Udoekwere UI, Kargo WJ. 2008. Trunk sensorimotor cortex is essential for autonomous weight-supported locomotion in adult rats spinalized as P1/P2 neonates. *J Neurophysiol*. 100:839–851.

Giszter SF, Hockensmith G, Ramakrishnan A, Udoekwere UI. 2010. How spinalized rats can walk: biomechanics, cortex, and hindlimb muscle scaling–implications for rehabilitation. *Ann N Y Acad Sci*. 1198:279–293.

Giszter SF, Kargo WJ, Davies M, Shibayama M. 1998. Fetal transplants rescue axial muscle representations in M1 cortex of neonatally transected rats that develop weight support. *J Neurophysiol*. 80:3021–3030.

Graziano MSA, Taylor CSR, Moore T. 2002. Complex movements evoked by microstimulation of precentral cortex. *Neuron*. 34:841–851.

Griffin DM, Hudson HM, Belhaj-Saif A, Cheney PD. 2014. EMG activation patterns associated with high frequency, long-duration intracortical microstimulation of primary motor cortex. *J Neurosci*. 34:1647–1656.

Hall RD, Lindholm EP. 1974. Organization of motor and somatosensory neocortex in the albino rat. *Brain Res*. 66:23–38.

Halley AC, Baldwin MKL, Cooke DF, Englund M, Krubitzer L. 2020. Distributed motor control of limb movements in rat motor and somatosensory cortex: the sensorimotor amalgam revisited. *Cereb Cortex*. 30:6296–6312.

Harkema S, Gerasimenko Y, Hodes J, Burdick J, Angeli C, Chen Y, Ferreira C, Willhite A, Rejc E, Grossman RG *et al*. 2011. Effect of epidural stimulation of the lumbosacral spinal cord on voluntary movement, standing, and assisted stepping after motor complete paraplegia: a case study. *Lancet*. 377:1938–1947.

Hekmatpanah J. 1961. Organization of tactile dermatomes, C1 through L4, in cat. *J Neurophysiol*. 24:129–140.

Hicks SP, D'Amato CJ. 1975. Motor-sensory cortex-corticospinal system and developing locomotion and placing in rats. *Am J Anat*. 143:1–42.

Hodges PW. 2001. Changes in motor planning of feedforward postural responses of the trunk muscles in low back pain. *Exp Brain Res*. 141:261–266.

Hooks BM. 2016. Sensorimotor convergence in circuitry of the motor cortex. *Neuroscientist*. 23:251–263.

Hooks BM, Mao T, Gutnisky DA, Yamawaki N, Svoboda K, Shepherd GMG. 2013. Organization of cortical and thalamic input to pyramidal neurons in mouse motor cortex. *J Neurosci*. 33:748–760.

Horak FB, Jacobs JV. 2007. Cortical control of postural responses. *J Neural Transm*. 114:1339–1348.

Humanes-Valera D, Aguilar J, Foffani G. 2013. Reorganization of the intact somatosensory cortex immediately after spinal cord injury. *PLoS One*. 8:e69655.

Hummelsheim H, Wiesendanger M. 1985. Is the hindlimb representation of the rat's cortex a "sensorimotor amalgam". *Brain Res*. 346:75–81.

Ingemanson ML, Rowe JR, Chan V, Wolbrecht ET, Reinkensmeyer DJ, Cramer SC. 2019. Somatosensory system integrity explains differences in treatment response after stroke. *Neurology*. 92:e1098–e1108.

Itomi K, Kakigi R, Maeda K, Hoshiyama M. 2000. Dermatome versus homunculus; detailed topography of the primary somatosensory cortex following trunk stimulation. *Clin Neurophysiol*. 111:405–412.

Kao T, Shumsky JS, Murray M, Moxon KA. 2009. Exercise induces cortical plasticity after neonatal spinal cord injury in the rat. *J Neurosci*. 29:7549–7557.

Karayannidou A, Zelenin PV, Orlovsky GN, Sirota MG, Beloozerova IN, Deliagina TG. 2009. Maintenance of lateral stability during standing and walking in the cat. *J Neurophysiol*. 101:8–19.

Kargo WJ, Nitz DA. 2003. Early skill learning is expressed through selection and tuning of cortically represented muscle synergies. *J Neurosci*. 23:11255–11269.

Kirk EJ. 1968. The dermatomes of the sheep. *J Comp Neurol*. 134:353–369.

Kirk EJ, Denny-Brown D. 1970. Functional variation in dermatomes in the macaque monkey following dorsal root lesions. *J Comp Neurol*. 139:307–320.

Knudsen EB, Moxon KA. 2017. Restoration of hindlimb movements after complete spinal cord injury using brain-controlled functional electrical stimulation. *Front Neurosci*. 11:715.

Kuhn RA. 1953. Organization of tactile dermatomes in cat and monkey. *J Neurophysiol*. 16:169–182.

Kunori N, Takashima I. 2016. High-order motor cortex in rats receives somatosensory inputs from the primary motor cortex via cortico-cortical pathways. *Eur J Neurosci*. 44:2925–2934.

Leergaard TB, Alloway KD, Pham TAT, Bolstad I, Hoffer ZS, Pettersen C, Bjaalie JG. 2004. Three-dimensional topography of corticopontine projections from rat sensorimotor cortex: comparisons with corticostriatal projections reveal diverse integrative organization. *J Comp Neurol*. 478:306–322.

Lemieux M, Josset N, Roussel M, Couraud S, Bretzner F. 2016. Speed-dependent modulation of the locomotor behavior in adult mice reveals attractor and transitional gaits. *Front Neurosci*. 10:42.

Lenschow C, Brecht M. 2018. Physiological and anatomical outputs of rat genital cortex. *Cereb Cortex*. 28:1472–1486.

Li CX, Waters RS. 1991. Organization of the mouse motor cortex studied by retrograde tracing and intracortical microstimulation (ICMS) mapping. *Can J Neurol Sci*. 18:28–38.

Lilja J, Endo T, Hofstetter C, Westman E, Young J, Olson L, Spenger C. 2006. Blood oxygenation level-dependent visualization of synaptic relay stations of sensory pathways along the neuroaxis in response to graded sensory stimulation of a limb. *J Neurosci*. 26:6330–6336.

Liu C, Foffani G, Scaglione A, Aguilar J, Moxon KA. 2017. Adaptation of thalamic neurons provides information about the spatiotemporal context of stimulus history. *J Neurosci*. 37:10012–10021.

Lombard MC, Nashold BS, Albe-Fessard D, Salman N. 1979. Deafferentation hypersensitivity in the rat after dorsal rhizotomy: a possible animal model of chronic pain. *Pain*. 6:163–174.

Manohar A, Flint RD, Knudsen E, Moxon KA. 2012. Decoding hindlimb movement for a brain machine interface after a complete spinal transection. *PLoS One*. 7:e52173.

Manohar A, Foffani G, Ganzer PD, Bethea JR, Moxon KA. 2017. Cortex-dependent recovery of unassisted hindlimb locomotion after complete spinal cord injury in adult rats. *Elife*. 6:e23532.

Mao T, Kusefoglu D, Hooks BM, Huber D, Petreanu L, Svoboda K. 2011. Long-range neuronal circuits underlying the interaction between sensory and motor cortex. *Neuron*. 72:111–123.

Megevand P, Troncoso E, Quairiaux C, Muller D, Michel CM, Kiss JZ. 2009. Long-term plasticity in mouse sensorimotor circuits after rhythmic whisker stimulation. *J Neurosci*. 29:5326–5335.

Morales-Botello ML, Aguilar J, Foffani G. 2012. Imaging the spatio-temporal dynamics of supragranular activity in the rat somatosensory cortex in response to stimulation of the paws. *PLoS One*. 7:e40174.

Moreno-López Y, Olivares-Moreno R, Cordero-Erausquin M, Rojas-Piloni G. 2016. Sensorimotor integration by corticospinal system. *Front Neuroanat*. 10:24.

Murray AJ, Croce K, Belton T, Akay T, Jessell TM. 2018. Balance control mediated by vestibular circuits directing limb extension or antagonist muscle co-activation. *Cell Rep*. 22:1325–1338.

Neafsey EJ, Bold EL, Haas G, Hurley-Gius KM, Quirk G, Sievert CF, Terreberry RR. 1986. The organization of the rat motor cortex: a microstimulation mapping study. *Brain Res Rev*. 11:77–96.

Nicholson C, Freeman JA. 1975. Theory of current source density analysis and determination of conductivity tensor for anuran cerebellum. *J Neurophysiol*. 38:356–368.

Overduin SA, d'Avella A, Carmena JM, Bizzi E. 2014. Muscle synergies evoked by microstimulation are preferentially encoded during behavior. *Front Comput Neurosci*. 8:20.

Oza CS, Giszter SF. 2014. Plasticity and alterations of trunk motor cortex following spinal cord injury and non-stepping robot and treadmill training. *Exp Neurol*. 256:57–69.

Oza CS, Giszter SF. 2015. Trunk robot rehabilitation training with active stepping reorganizes and enriches trunk motor cortex representations in spinal transected rats. *J Neurosci*. 35:7174–7189.

Paxinos G, Watson C. 2007. *The rat brain in stereotaxic coordinates*. 6th ed. San Diego (CA): Academic Press.

Pettersen KH, Devor A, Ulbert I, Dale AM, Einevoll GT. 2006. Current-source density estimation based on inversion of electrostatic forward solution: effects of finite extent of

neuronal activity and conductivity discontinuities. *J Neurosci Methods*. 154:116–133.

Ramanathan D, Conner JM, Tuszynski MH. 2006. A form of motor cortical plasticity that correlates with recovery of function after brain injury. *Proc Natl Acad Sci USA*. 103:11370–11375.

Rejc E, Angeli CA, Atkinson D, Harkema SJ. 2017. Motor recovery after activity-based training with spinal cord epidural stimulation in a chronic motor complete paraplegic. *Sci Rep*. 7:1–12.

Rosén I, Asanuma H. 1972. Peripheral afferent inputs to the forelimb area of the monkey motor cortex: input-output relations. *Exp Brain Res*. 14:257–273.

Rossignol S, Dubuc R, Gossard J-P. 2006. Dynamic sensorimotor interactions in locomotion. *Physiol Rev*. 86:89–154.

Seelke AMH, Dooley JC, Krubitzer LA. 2012. The emergence of somatotopic maps of the body in s1 in rats: the correspondence between functional and anatomical organization. *PLoS One*. 7:e32322.

Sherrington CS. 1892. Experiments in examination of the peripheral distribution of the fibres of the posterior roots of some spinal nerves. *Proc R Soc London*. 52:333–337.

Smith CL. 1986. Sensory neurons supplying touch domes near the body midlines project bilaterally in the thoracic spinal cord of rats. *J Comp Neurol*. 245:541–552.

Smith JB, Alloway KD. 2013. Rat whisker motor cortex is subdivided into sensory-input and motor-output areas. *Front Neural Circuits*. 7:4.

Song W, Cajigas I, Brown EN, Giszter SF. 2015. Adaptation to elastic loads and BMI robot controls during rat locomotion examined with point-process GLMs. *Front Syst Neurosci*. 9:62.

Stepniewska I, Fang P-C, Kaas JH. 2005. Microstimulation reveals specialized subregions for different complex movements in posterior parietal cortex of prosimian galagos. *Proc Natl Acad Sci USA*. 102:4878–4883.

Takahashi Y, Nakajima Y, Sakamoto T. 1994. Dermatome mapping in the rat hindlimb by electrical stimulation of the spinal nerves. *Neurosci Lett*. 168:85–88.

Takeoka A, Vollenweider I, Courtine G, Arber S. 2014. Muscle spindle feedback directs locomotor recovery and circuit reorganization after spinal cord injury. *Cell*. 159:1626–1639.

Tandon S, Kambi N, Jain N. 2008. Overlapping representations of the neck and whiskers in the rat motor cortex revealed by mapping at different anaesthetic depths. *Eur J Neurosci*. 27:228–237.

Tandon S, Kambi N, Mohammed H, Jain N. 2013. Complete reorganization of the motor cortex of adult rats following long-term spinal cord injuries. *Eur J Neurosci*. 38:2271–2279.

Tsao H, Galea MP, Hodges PW. 2008. Reorganization of the motor cortex is associated with postural control deficits in recurrent low back pain. *Brain*. 131:2161–2171.

Tsao H, Tucker KJ, Hodges PW. 2011. Changes in excitability of corticomotor inputs to the trunk muscles during experimentally-induced acute low back pain. *Neuroscience*. 181:127–133.

Tutunculer B, Foffani G, Himes BT, Moxon KA. 2006. Structure of the excitatory receptive fields of infragranular forelimb neurons in the rat primary somatosensory cortex responding to touch. *Cereb Cortex*. 16:791–810.

Van Den Brand R, Heutschi J, Barraud Q, DiGiovanna J, Bartholdi K, Huerlimann M, Friedli L, Vollenweider I, Moraud EM, Duis S *et al*. 2012. Restoring voluntary control of locomotion after paralyzing spinal cord injury. *Science (80-)*. 336:1182–1185.

Welker C. 1971. Microelectrode delineation of fine grain somatotopic organization of SmI cerebral neocortex in albino rat. *Brain Res*. 26:259–275.

Wessels WJT, Feirabend HKP, Marani E. 1994. The rostrocaudal organization in the dorsal root ganglia of the rat : a consequence of plexus formation? *Anat Embryol (Berl)*. 190:1–11.

Whelan PJ. 2009. The involvement of the motor cortex in postural control: a delicate balancing act. *J Physiol*. 587:3753.

Xerri C, Stern J, Merzenich M. 1994. Alterations of the cortical representation of the rat ventrum induced by nursing behavior. *J Neurosci*. 14:1710–1721.

Yagüe JG, Humanes-Valera D, Aguilar J, Foffani G. 2014. Functional reorganization of the forepaw cortical representation immediately after thoracic spinal cord hemisection in rats. *Exp Neurol*. 257:19–24.

Young NA, Vuong J, Flynn C, Teskey GC. 2011. Optimal parameters for microstimulation derived forelimb movement thresholds and motor maps in rats and mice. *J Neurosci Methods*. 196:60–69.